

Nonuniform Upwelling in a Shallow-Water Model of the Antarctic Bottom Water in the Brazil Basin*

OLIVIER MARCHAL

Department of Geology and Geophysics, Woods Hole Oceanographic Institution, Woods Hole, Massachusetts

JONAS NYCANDER

Department of Meteorology, University of Stockholm, Stockholm, Sweden

(Manuscript received 25 June 2003, in final form 21 May 2004)

ABSTRACT

A numerical model based on the shallow-water equations is developed to represent the flow of Antarctic Bottom Water (AABW) in the Brazil Basin (southwest Atlantic Ocean). The aim is twofold. First, an attempt is made to identify in a model that includes both simplified dynamics and realistic bathymetry (at $1/6^\circ$ resolution) the impacts of the elevated diapycnal mixing rates near the Mid-Atlantic Ridge (MAR) documented by dissipation data of the Deep Basin Experiment (DBE). To this end, different assumptions regarding the distribution of the velocity across the AABW layer interface (w) are considered. Second, the extent to which the shallow-water model can replicate observations relative to AABW circulation in the basin, in particular the trajectory and velocity of neutrally buoyant floats released in the AABW during the DBE, is examined. The model flows are characterized by small Rossby numbers, except in the northward-flowing western boundary current where kinetic energy is largely concentrated. To interpret the flows, model streamlines are compared with isopleths of linear potential vorticity f/h_0 of the shallow-water theory (f is the planetary vorticity and h_0 is the layer thickness in the absence of motion). The f/h_0 contours are oriented northwest–southeast in the western part of the basin and southwest–northeast in the eastern part, reflecting the bowl-shaped topography of the Southern Hemisphere basin. With a spatially uniform (positive) w , the ubiquitous vortex stretching produces a flow to the southeast, consistent with the Stommel–Arons theory. This flow occurs in most of the basin interior, even in the east where f/h_0 contours converge to the northeastern end of the basin. With strongly positive w near the ridge and zero or slightly negative w elsewhere, the flow follows more closely f/h_0 contours in the western interior and intersects them near the ridge. The confinement of the diapycnal mass flux near the MAR drastically reduces the southward flow in the interior or even reverses its direction, leading to a circulation quite distinct from that of the Stommel–Arons theory. The model results compare favorably to some (but not all) hydrographic estimates of AABW circulation patterns and rates. On the other hand, the model streamlines and velocities show important differences with, respectively, the trajectory and the velocity of the floats launched in the AABW layer. The prescription of vanishing w in the interior does not systematically improve the fit of the model streamlines to the float trajectories, and the model velocities simulated with spatially uniform w or spatially variable w are on average smaller by one order of magnitude than the float velocities. A variety of mechanisms, which are not included in the numerical experiments, may explain the differences between the model results and the float data.

1. Introduction

The abyssal circulation refers to the water motions below the base of the main thermocline (at a depth of ~ 1 km). Whereas it volumetrically dominates the ocean general circulation, our theoretical understanding of the mean circulation in the abyss remains incomplete (Ped-

losky 1996). Stommel and Arons (1960) developed a theoretical picture of the abyssal circulation that still dominates modern ideas about the mean flow in the subthermocline region. They assumed geostrophy to study the dynamics of a layer of incompressible and homogeneous fluid on a flat-bottom sphere rotating with the earth's angular velocity and including meridional solid boundaries. A distributed velocity across the layer interface (hereinafter w), which is not specified by the theory and balances localized deep water sources, forces the motion in the layer. Assuming a spatially uniform (positive) value for w , two major predictions of the Stommel–Arons theory are (i) a poleward and eastward flow in the interior produced by vortex stretching, and (ii) the existence of a deep western boundary current

* Woods Hole Oceanographic Institution Contribution Number 11161.

Corresponding author address: Dr. Olivier Marchal, Department of Geology and Geophysics, Woods Hole Oceanographic Institution, Woods Hole, MA 02543.
E-mail: omarchal@whoi.edu

(DWBC). The support for the theory seems to come mostly from the observation of DWBCs (for early studies see, e.g., Wüst 1935; Swallow and Worthington 1957), even though only the existence, not the dynamical nature, of the current is determined by the theory. Early attempts to directly measure the mean circulation in the abyssal interior, which is the object of the theory, were spoiled by the presence of an unexpectedly large mesoscale eddy activity (Crease 1962; Swallow 1971).

Direct measurement of the mean circulation in an abyssal basin was more recently reattempted in the framework of the Deep Basin Experiment (DBE; Hogg et al. 1996), a component of the World Ocean Circulation Experiment. A total number of 168 neutrally buoyant floats with intended duration of 60–800 days were released at ~2500 and 4000 m in the Brazil Basin, with the expectation that the mean circulation would be revealed through averaging out the eddy motions (Hogg and Owens 1999). A major result of the study was the indication of zonal motions with small meridional scales in the interior, contrasting with previous inference from hydrographic data (e.g., Reid 1989; Demadron and Weatherly 1994) and with prediction by the Stommel–Arons theory.

Hogg and Owens (1999) hypothesized that the zonality observed in some of the float trajectories could be related to the enhanced diapycnal mixing observed near the Mid-Atlantic Ridge (MAR). Large insight into the distribution of diapycnal mixing in the abyssal Brazil Basin was provided by microstructure and tracer dispersion data obtained as part of the DBE (e.g., Polzin et al. 1997; Ledwell et al. 2000; St. Laurent et al. 2001). Microstructure velocity data were used to estimate rates of dissipation of turbulent kinetic energy (TKE). These estimates were then combined with buoyancy frequency data to infer diapycnal eddy diffusivities for mass (k_ρ) on the basis of a simplified model of turbulence (Osborn 1980). The estimated diffusivity levels are weak at all depths above smooth abyssal plains and the South American Continental Rise, amounting to less than or approximately equal to $10^{-5} \text{ m}^2 \text{ s}^{-1}$; in contrast, the levels are large throughout the water column above the rough MAR, with values for the bottommost 150 m exceeding $5 \times 10^{-4} \text{ m}^2 \text{ s}^{-1}$ (Polzin et al. 1997). Data of tracer dispersion and velocity microstructure imply diffusivities of $2\text{--}4 \times 10^{-4} \text{ m}^2 \text{ s}^{-1}$ at 500 m above abyssal hills on the western flank of the MAR and about $10 \times 10^{-4} \text{ m}^2 \text{ s}^{-1}$ nearer the bottom (Ledwell et al. 2000). The horizontal variations in diapycnal mixing in the abyssal Brazil Basin appear therefore linked to the roughness of the bathymetry. Within the area of elevated roughness, maximum TKE levels occur on average over a sloping bottom; smaller levels were found above crests and canyons (St. Laurent et al. 2001).

The horizontal variations in diapycnal mixing should have important consequences for the circulation of the Antarctic Bottom Water (AABW) in the Brazil Basin. The AABW is the only water below ~3700 m in the

basin (e.g., Demadron and Weatherly 1994; Morris et al. 2001). It enters the basin through the Vema Channel (Hogg et al. 1999) and the Hunter Channel (Zenk et al. 1999), and exits the basin through the Romanche–Chain Fracture Zones (FZs; Mercier and Speer 1998) and a zonal passage situated at $\sim 36^\circ\text{W}$ at the equator (Hall et al. 1997; Fig. 1). Volume fluxes of AABW through these constrictions estimated by direct current measurement and geostrophic computation indicate that a flux of $\sim 3.7 \text{ Sv}$ ($1 \text{ Sv} \equiv 10^6 \text{ m}^3 \text{ s}^{-1}$) must upwell across the upper surface of the AABW in order to balance the net inflow of the water into the basin (Table 1). Morris et al. (2001) estimated the average k_ρ across neutral density surfaces within the AABW, based on AABW inflows and outflows at the basin rims in different potential temperature classes and on an empirical relationship between bathymetric roughness and TKE dissipation deduced from dissipation data (St. Laurent et al. 2001). The average k_ρ was estimated to $1\text{--}5 \times 10^{-4} \text{ m}^2 \text{ s}^{-1}$, consistent with previous values of $3\text{--}4 \times 10^{-4} \text{ m}^2 \text{ s}^{-1}$ obtained from a less extensive dataset (Hogg et al. 1982). The available microstructure data suggest that these levels do not occur uniformly but are confined in the vicinity of the MAR (Polzin et al. 1997; Ledwell et al. 2000; St. Laurent et al. 2001). Closure of the AABW mass budget would thus be largely achieved through mixing in only a subregion of the basin, contrasting with the perception of quasi-uniform upwelling in the subthermocline region. Note that enhanced diapycnal mixing over the midocean ridge may occur in other basins. Mauritzen et al. (2002) inferred, from anomalies in the salinity, oxygen, and nutrient fields, that diapycnal mixing is enhanced over the western flank of the ridge in the North Atlantic.

In this paper we develop a shallow-water model of the circulation of AABW in the Brazil Basin. Shallow-water models have become a common tool to enhance understanding of the abyssal circulations (e.g., Kawase and Straub 1991; Hallberg and Rhines 1996; Edwards and Pedlosky 1998; Yang and Price 2000). They also constitute the building block of isopycnal models of the ocean general circulation, in which the ocean is viewed as a stack of layers, each of which has a constant density and is governed by equations resembling the shallow-water equations. Our aim is twofold. First, we attempt to explore in the shallow-water dynamical framework the impacts of the horizontal variations in diapycnal mixing documented by dissipation data. In particular, we examine the dynamically important hypothesis that enhanced diapycnal mixing near the MAR could contribute to the zonal character of the trajectory of some of the floats launched in the AABW during the DBE (Hogg and Owens 1999). Second, we attempt to assess the extent to which the shallow-water model can capture observations relative to the abyssal circulation in a particular basin that has been relatively well studied. Previous works used the shallow-water model to simulate bottom water circulation in basins with realistic topog-

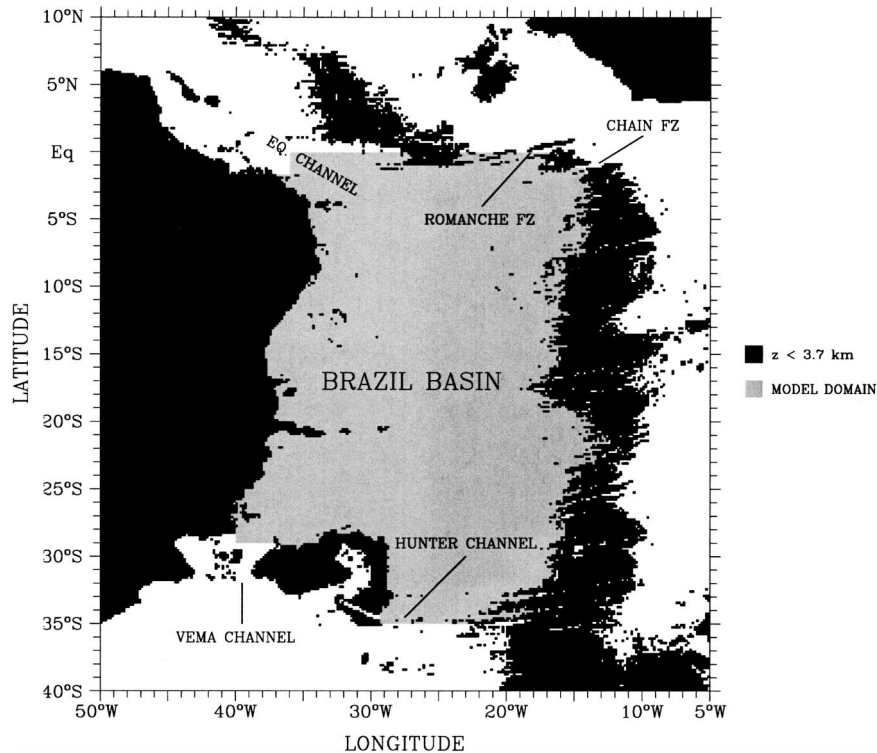


FIG. 1. Some major bathymetric features of the Brazil Basin and model domain. The bathymetric data come from satellite altimetry and ship depth soundings (Smith and Sandwell 1997). The raw data, available at $2' \times 2'$ resolution, have been arithmetically averaged in grid cells of $10' \times 10'$ to produce the figure. The model domain comprises grid cells in the Brazil Basin with a depth $z > 3700$ m.

raphy (e.g., Stephens and Marshall 2000; Curchitser et al. 2001). Confidence in the model would be increased if it can be shown that the model can replicate at least some of the features constrained by observations (see also Stephens and Marshall 2000).

It is worth being explicit about the limitations of the present study. Perhaps the greatest drawback is the omission of any dynamical interaction of the bottom layer with the overlying layers except through the cross-interface velocity w . The view is adopted that the motion in the bottom layer is forced exclusively by the mechanism of vortex stretching and compression provided by w . A second shortcoming of the model is the lack of density stratification to study the bottom water dynamics. Thus, the assumption is made that the circulation of AABW in the Brazil Basin does not depend

in a crucial way on the stratification within the layer. A positive aspect of the model, however, is that it provides a simple dynamical framework that can be used in conjunction with realistic topography, so that progress toward understanding the impacts of the horizontal variations of diapycnal mixing in the real ocean can be made. In order to isolate these impacts, the model neglects other factors that might potentially influence the AABW circulation in the Brazil Basin and the trajectory of neutrally buoyant floats in particular (section 5b).

Previous model studies addressed the dynamical impacts of spatial variations in diapycnal mixing in the Brazil Basin (Spall 2001; St. Laurent et al. 2001; Huang and Jin 2002). Spall (2001) configured a nonlinear, planetary geostrophic model to represent a region of mixing over the MAR in the southeastern part of the

TABLE 1. Lateral boundary conditions of the model.

Region	Lon	Lat	Flux* (Sv)	Reference
Vema Channel	39°00'–37°10'W	29°00'S	4.0	Hogg et al. (1999)
Hunter Channel	28°00'–27°10'W	35°00'S	2.9	Zenk et al. (1999)
Equatorial Channel	36°00'W	1°40'S–0°00'	–2.0	Hall et al. (1997)
Romanche FZ	19°00'–18°00'W	0°00'	–0.6	Mercier and Speer (1998)
Chain FZ	15°00'–14°00'W	1°10'S	–0.6	Mercier and Speer (1998)

* Positive values denote net inflow of AABW into the Brazil Basin.

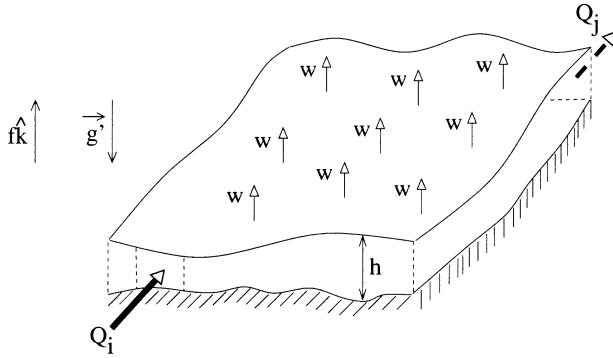


FIG. 2. Schematic representation of the shallow-water model. A layer of incompressible and homogeneous fluid resides on a variable rigid bottom rotating with the earth angular velocity with local vertical component = $f\mathbf{k}/2$, where \mathbf{k} is a vertical unit vector. The layer, with local thickness h , receives a net volume flux $Q_i - Q_j$ that is balanced by a velocity w at its upper surface. The layer is subjected to an effective gravity g' .

basin. St. Laurent et al. (2001) combined hydrographic and TKE dissipation data with an inverse model using both beta-spiral and the integrated forms of the advective budgets of heat and mass to constrain the circulation in this region. Huang and Jin (2002) used a z -coordinate primitive equation (PE) model of the south Atlantic Ocean to study the effects of bottom-intensified mixing over the MAR. All of these studies concluded that the presence of localized diapycnal mixing may have a profound influence on the abyssal circulation. The present work differs from these previous studies by (i) focusing specifically on the circulation of AABW in the whole basin using a model with relatively high spatial resolution, and (ii) comparing quantitatively model results with observational estimates of the abyssal circulation, in particular with estimates based on float data.

The paper is organized as follows. Section 2 describes the numerical model—that is, the shallow-water equations, the method of solution, and the model parameters. Steady-state solutions corresponding to spatially uniform and spatially variable w , which parameterizes buoyancy forcing due to unresolved diabatic mixing processes, are compared in section 3. A dynamical interpretation of the numerical results is given. In section 4 the results of the shallow-water model are compared with estimates of the circulation of AABW in the Brazil Basin inferred from observations and from previous models. Our results, in particular the comparison between the model and float data, are discussed in section 5. Conclusions follow in section 6.

2. Numerical model

a. Shallow-water equations

We consider the dynamics of a layer of incompressible and homogeneous fluid described in a frame rotating with the earth angular velocity (Fig. 2). The layer in our case is identified as the AABW resting on the

bottom of the Brazil Basin. The effects of the internal stratification within the bottom layer and of the circulation in the upper layer are excluded. The equations of motion for the layer are the shallow-water equations:

$$\frac{\partial \mathbf{u}}{\partial t} + q\mathbf{k} \times \mathbf{u}h = -\nabla(\Phi + K) + \mathbf{F} \quad \text{and} \quad (1)$$

$$\frac{\partial h}{\partial t} + \nabla \cdot (\mathbf{u}h) = -w, \quad (2)$$

where t is time, \mathbf{u} is the (horizontal) velocity vector, \mathbf{k} is a vertical unit vector, $q = (\zeta + f)/h$ is the potential vorticity (PV), $\zeta = \mathbf{k} \cdot (\nabla \times \mathbf{u})$ is the (vertical component of) relative vorticity, f is the (vertical component of) planetary vorticity, $h = h_0 + \eta$ is the fluid layer thickness, $h_0(\mathbf{r})$ is the thickness in the absence of motion, η is the free surface perturbation, $\Phi = g'\eta$ is the geopotential at the free surface, g' is the reduced gravity, $K = |\mathbf{u}|^2/2$ is the (horizontal) kinetic energy per unit mass, w is the velocity across the layer interface, and \mathbf{F} is the friction force per unit mass. Both Ekman friction and horizontal diffusion of momentum are considered:

$$\mathbf{F} = -\sqrt{\frac{A_v |f|}{2}} \frac{\mathbf{u}}{h} + \frac{A_h}{h} \nabla \cdot (h \nabla \mathbf{u}), \quad (3)$$

where A_v and A_h are vertical and horizontal eddy viscosities.

Equations (1)–(2) are integrated with the following boundary conditions:

$$\mathbf{u} \cdot \mathbf{n} = 0 \quad \text{and} \\ \mathbf{u} \cdot \mathbf{t} = 0 \quad (\text{closed boundaries}), \quad (4)$$

$$\mathbf{u} \cdot \mathbf{n} = \pm u_0 \quad \text{and} \\ \mathbf{u} \cdot \mathbf{t} = 0 \quad (\text{open boundaries}), \quad (5)$$

where \mathbf{n} and \mathbf{t} are unit vectors normal and tangent to the boundary, respectively, and u_0 is the specified velocity component normal to the open boundary. The condition $\mathbf{u} \cdot \mathbf{n} = \pm u_0$ is intended to represent inflows or outflows of AABW at the few passages around the basin. The boundary conditions imply at steady state a balance between the net inflow into the layer and the upwelling at the top of the layer:

$$\sum_i Q_i = \iint_A w \, dA, \quad (6)$$

where $Q_i = (hu_0 \Delta r)_i$ is the volume flux at the i th open boundary (positive if the flux is directed into the layer and negative if it is directed out of the layer), Δr_i is the width of the i th open boundary, and A is the total surface area of the basin.

b. Method of solution

We seek to determine the steady state flow in the layer, subjected to appropriate conditions at its lateral bound-

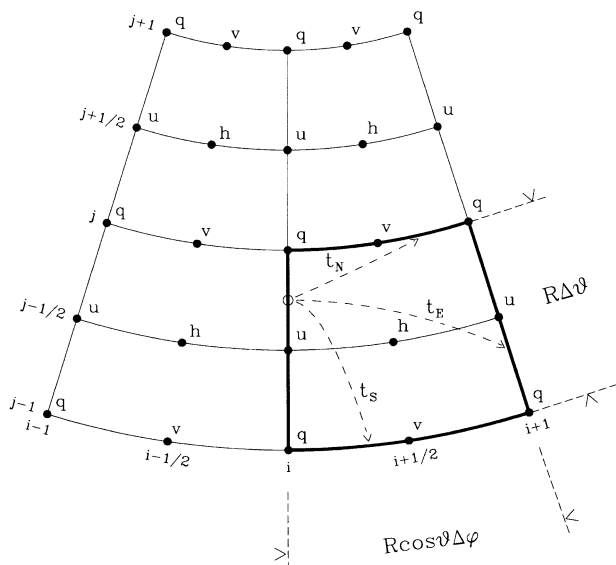


FIG. 3. Grid used for the potential enstrophy and energy-conserving scheme. Here R , φ , and ϑ denote the earth radius, longitude, and latitude, respectively. To illustrate the determination of model streamlines we consider a hypothetical water particle located on the meridional boundary of the cell $(u_{i,j-1/2}, v_{i+1/2,j}, u_{i+1,j-1/2}, v_{i+1/2,j-1})$ (open circle). If $u_{i,j-1/2} > 0$ the particle follows one of three possible trajectories, corresponding to a displacement to the northern boundary (in time t_N), eastern boundary (t_E), or southern boundary (t_S). In case of local mass convergence—that is, $u_{i,j-1/2} > 0$, $v_{i+1/2,j} < 0$, $u_{i+1,j-1/2} < 0$, and $v_{i+1/2,j-1} > 0$ —the particle “disappears” in the cell.

aries. To this end, Eqs. (1)–(2) are integrated numerically to steady state with boundary conditions (4)–(5). The equations are discretized on a spherical grid using a finite-difference scheme that is second-order accurate and conserves potential enstrophy and energy (Arakawa and Lamb 1981). The grid is a staggered Arakawa C grid with a size of $10'$ in longitude and latitude (Fig. 3). The metric terms arising from the discretization of horizontal momentum diffusion on the spherical grid are neglected, since this is only an arbitrary parametrization of dissipation. Apart from the dissipation parametrization, all the metric terms due to motion on a sphere are retained (Arakawa and Lamb 1981). Equations (1)–(2) are time integrated using the explicit, third-order Runge–Kutta scheme; a low-storage variant of the scheme is employed (Williamson 1980). The Ekman friction, however, is fully implicit.

The model domain comprises the area within the 3700-m isobath in the Brazil Basin (shaded area in Fig. 1). This value is approximately equal to the mean depth of the 2.0°C potential temperature isotherm in the basin, which we take as the boundary between AABW and the overlying North Atlantic Deep Water (e.g., Speer and Zenk 1993) and which we estimate from two different meridional sections (Fig. 3 of Demadron and Weatherly 1994; Fig. 4 of Morris et al. 2001). The model bathymetry comes from a compilation of satellite altimetry and ship sounding data. (Smith and Sandwell 1997). The

bathymetric data at $2' \times 2'$ resolution have been arithmetically averaged in model grid cells of $10' \times 10'$. Note that the algorithm to convert gravimetry to bathymetry has a fundamental resolution limit of π times the mean ocean depth, that is, about 12 km (Sandwell et al. 2003). This is less than but comparable to the model grid size of ~ 19 km in longitude.

The numerical implementation of the boundary conditions is as follows. The grid is arranged so that the meridional and zonal boundaries of the basin and of the “islands” within the domain carry the u and v grid points, respectively. Open boundaries occur at the five bathymetric constrictions through which AABW flows have been observed (Fig. 1 and Table 1). The velocity component normal to the open boundary u_0 is obtained by dividing an observational estimate of AABW volume flux through the boundary (Table 1) by the corresponding sectional area. This area is calculated from (i) the longitudinal or latitudinal range of the boundary (Table 1) and (ii) a layer thickness value constrained from local bathymetry and the assumption that the top of AABW is at 3700 m. Thus the u_0 values are time-invariant. The discretization of the term $q\mathbf{k} \times \mathbf{u}\mathbf{h}$ in the momentum equation requires the specification of PV values at the (open and closed) boundaries (Arakawa and Lamb 1981). To permit a gradient of relative vorticity near the boundaries, ζ at the meridional and zonal boundary is calculated from a linear extrapolation of the nearest v and u value within the domain, respectively, using the no-slip condition $\mathbf{u} \cdot \mathbf{t} = 0$ at the boundary.

We note that our treatment of closed boundaries does not allow the free surface to occupy new grid cells or to retire along a sloping bottom (“vertical walls” are assumed). Different approaches are available to represent numerically the contact of free surfaces with sloping boundaries in isopycnic models (for a short review see, e.g., Hsu and Arakawa 1990; Sielicki and Wurtele 1970). Although the implementation of some of these approaches has been an important part of the development of the model, the idealized boundary conditions in Eq. (4) are adopted in the present study. To avoid numerical instabilities arising from the simulation of very thin layers, we remove from the computational domain any grid cell for which h drops below a critical value and then apply the conditions in Eq. (4) along the boundaries of the cell. In the experiments reported in this study we use a critical value of 1 m, which results in the removal of a small fraction of the initial number of “wet” cells (1%–3%).

c. Parameter values

The model includes four parameters: the reduced gravity g' , the eddy viscosities A_v and A_h , and the cross-interface velocity w (Table 2). A reduced gravity $g' = 1.7 \times 10^{-3} \text{ m s}^{-2}$ is assumed. This value is consistent with the mean buoyancy frequency profile along 25°W in the abyssal Brazil Basin reported by Thurnherr and Speer (2003, their Fig. 9) and is identical to the value

TABLE 2. Reference value of the model parameters.

Parameter	Symbol	Value	Units
Reduced gravity	g'	1.7×10^{-3}	m s^{-2}
Vertical eddy viscosity	A_v	10^{-2}	$\text{m}^2 \text{s}^{-1}$
Horizontal eddy viscosity	A_h	10^3	$\text{m}^2 \text{s}^{-1}$
Cross-interface velocity	w	4.8×10^{-7}	m s^{-1}

used by Stephens and Marshall (2000) to simulate AABW circulation in the whole Atlantic. Unless stated otherwise the values used for A_v and A_h are $10^{-2} \text{ m}^2 \text{ s}^{-1}$ and $10^3 \text{ m}^2 \text{ s}^{-1}$, respectively. The first value corresponds to an Ekman layer thickness $\delta_E = (2A_v/f)^{1/2} = 21 \text{ m}$ at a latitude of 17.5° (the midlatitude of our basin). The second value corresponds to a Munk layer thickness $\delta_M = (A_h/\beta)^{1/3} = 36 \text{ km}$ at the same latitude (β is the planetary vorticity gradient). The sensitivity of model results to the values assumed for A_v and A_h will be explored. Different spatial distributions of the cross-interface velocity w (representing buoyancy forcing) will be considered, which constitutes the focus of the study.

3. Model results

a. Distribution of f/h_0

The divergent nature of the flow field at steady state, $\nabla \cdot (\mathbf{u}h) = -w$, precludes using a streamfunction as simply defined as $\mathbf{u} = \mathbf{k} \times \nabla\psi$ to describe the model flows. To describe these flows we use streamlines. Streamlines are calculated analytically from the model velocity fields using the approach of Döös (1995; our appendix). They will be compared with f/h_0 isopleths in order to interpret the numerical results. Combining Eqs. (1)–(2) gives the equation of potential vorticity for the layer. At steady state,

$$h\mathbf{u} \cdot \nabla q = wq + \mathbf{k} \cdot (\nabla \times \mathbf{F}). \quad (7)$$

The advective transport of potential vorticity is balanced by the flux of PV at the top of the layer owing to upwelling and by the dissipation of PV owing to frictional torque. For a flow with small Rossby number,

$$h\mathbf{u} \cdot \nabla \frac{f}{h_0} = w \frac{f}{h_0} + \mathbf{k} \cdot (\nabla \times \mathbf{F}). \quad (8)$$

This equation states the well-known result that a barotropic flow that is strictly in geostrophic balance ($w = 0$ and $\mathbf{F} = 0$) will be in line with f/h_0 isopleths. Comparing the streamlines and f/h_0 isopleths therefore gives information about the net effect of the diapycnal flux and dissipation of PV.

The f/h_0 contours are oriented northwest–southeast in the western part of the basin and southwest–northeast in the eastern part, reflecting the bowl-shaped topography of the basin and its location in the Southern Hemisphere (black lines in Fig. 4). The contours in the eastern part show small-scale structures associated with increased topographic roughness near the MAR. Small

topographic scales, however, are often irrelevant even for barotropic flows (Bretherton and Haidvogel 1976). At these scales f/h_0 isopleths may thus depart substantially from the streamlines of a barotropic flow that is precisely geostrophic. Note that our linear potential vorticity differs from the potential vorticity $(f/\sigma)\partial\sigma/\partial z$ calculated by O'Dwyer and Williams (1997), by omitting stratification and by including explicitly the contribution of bottom topographic gradients. This precludes a consistent comparison between our PV distribution and theirs for the Brazil Basin.

b. Experiments with uniform w

We first consider a reference experiment with a spatially uniform w and the value for the other model parameters listed in Table 2. The wording “reference” does not mean that this is the most realistic simulation but that the simulation functions as a pivot for sensitivity experiments. The spatially uniform w balancing the net inflow of 3.7 Sv at the rims of the basin (Table 1) amounts to $4.8 \times 10^{-7} \text{ m s}^{-1}$. This value is consistent with the estimated average upwelling rates of $(4\text{--}11) \times 10^{-7} \text{ m s}^{-1}$ for neutral density surfaces within the AABW (Morris et al. 2001, their Table 3b). This is expected because these authors and we rely on AABW volume fluxes from the same observational studies.

The model velocity field shows that kinetic energy is mostly confined to a northward-flowing western boundary current (Fig. 5). The maximum velocity amplitudes in the current are $O(10^{-1}) \text{ m s}^{-1}$ (Fig. 5), that is, much larger than the amplitudes in the interior, which are $O(10^{-3} - 10^{-2}) \text{ m s}^{-1}$ (Fig. 6). The velocity field in the interior is complex (Fig. 6). It is dominated by (i) a recirculation just east of the western boundary current and (ii) the outflows at the model Romanche–Chain FZs. To elucidate the circulation structure in the interior, we consider several streamlines distributed throughout the basin (Figs. 5, 6). In the western part of the basin and east of the western boundary current, the flow roughly is from the northwest to the southeast. In the eastern part, streamlines either converge to the model Romanche–Chain FZs, where net outflows are prescribed, or have the same orientation as in the west. In this latter case the streamlines end at the model ridge.

To help in interpreting the model circulation we first compare the distribution of the potential vorticities q and f/h_0 (blue and black lines, respectively, in Fig. 4). The two distributions are very similar except in the western boundary current. This indicates that the simulated flow has small Rossby numbers, except in the western boundary current where the advective nonlinearity is important. Hence, departures between streamlines and f/h_0 contours can generally be interpreted in terms of the net effect of diapycnal flux and dissipation of PV [Eq. (8)]. Second, we consider three streamlines whose initial location is close to selected f/h_0 contours at 30°W in the western part of the basin (blue lines in

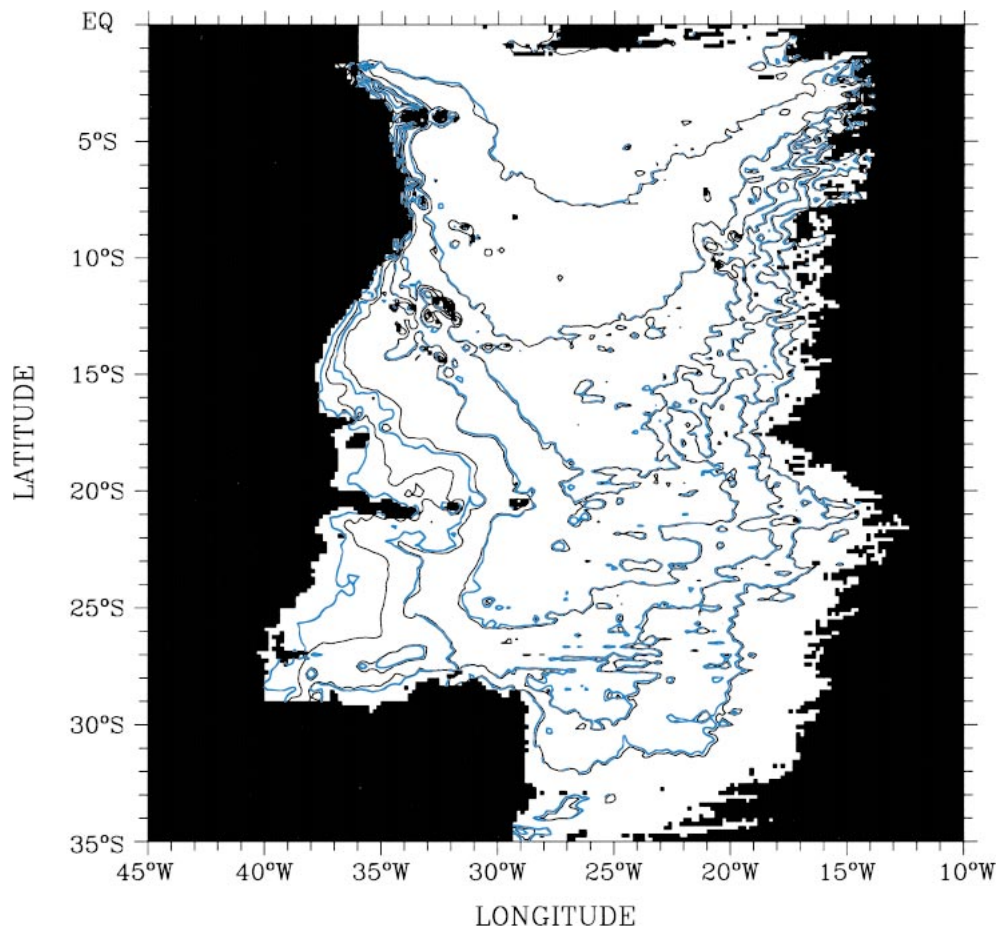


FIG. 4. Isopleths of the potential vorticities f/h_0 (black) and q (blue) for the AABW layer in the Brazil Basin. The f/h_0 values have been calculated assuming that the top of the layer is at a depth of 3700 m. The q values are for the reference experiment.

Fig. 7). All streamlines deviate southward from their corresponding f/h_0 isopleth and intersect many f/h_0 contours in the eastern part of the basin. This indicates that the interior flow in the model is strongly affected by the diapycnal flux and dissipation of PV.

To assess the relative importance of dissipation in the model, we consider an experiment with the same parameter values as the reference experiment except that the vertical and horizontal viscosities are reduced by a factor of 2, that is, $A_v = 0.5 \times 10^{-2} \text{ m}^2 \text{ s}^{-1}$ and $A_h = 0.5 \times 10^3 \text{ m}^2 \text{ s}^{-1}$. These values correspond to boundary layer thicknesses $\delta_E = 15 \text{ m}$ and $\delta_M = 28 \text{ km}$, respectively, at the midlatitude of the basin. The streamlines in the interior (red lines in Fig. 7) are very close to those of the reference experiment. We thus conclude that the diapycnal flux, not the dissipation, is the dominant term that balances the transport of PV in the interior [Eq. (8)]. The dynamical nature of the flow in the interior is essentially the same as in the Stommel–Arns theory, except for the northern part of the basin where the circulation is affected by the outflows at the Romanche–Chain FZs (Fig. 6).

c. Experiments with variable w

We now consider sensitivity experiments with a spatially variable w . Although the distribution of the velocity across the AABW “interface” in the Brazil Basin is largely unknown, the turbulent dissipation data obtained as part of the DBE did provide valuable insight. Consider the following balance in the density equation (e.g., St. Laurent et al 2001):

$$w_* N^2 = -\frac{\partial J_\rho}{\partial z}, \quad (9)$$

where w_* is the diapycnal velocity, N is the buoyancy frequency, J_ρ is the turbulent flux of buoyancy, and z is the vertical coordinate. The diapycnal advection is the vertical component of flow through isopycnals, associated with a convergence of the buoyancy flux J_ρ (St. Laurent et al. 2001). The balance in Eq. (9) assumes steady state and neglects lateral fluxes of buoyancy, as well as cabbeling and thermobaricity (McDougall 1987). Using the eddy closure $J_\rho = -k_\rho N^2$ and the TKE model $k_\rho = \Gamma \epsilon / N^2$ (Osborn 1980), where Γ is the mixing effi-

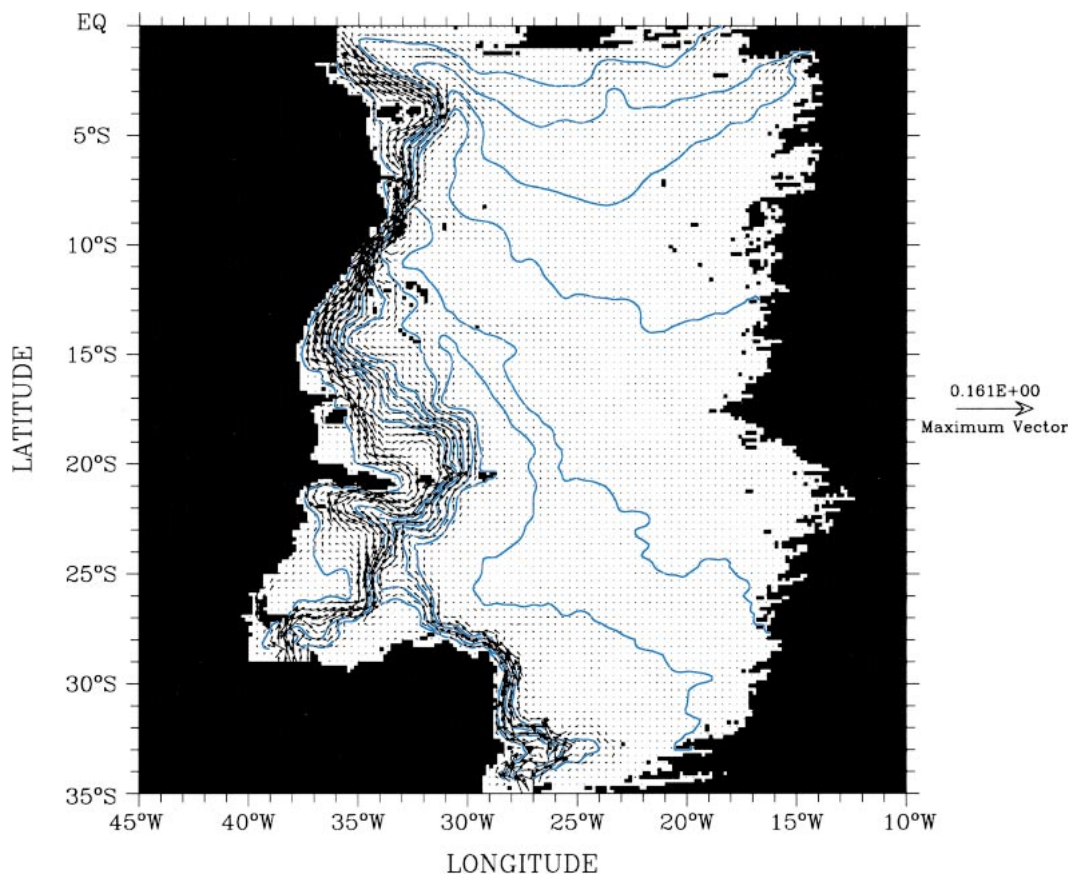


FIG. 5. Velocity field (in m s^{-1}) and selected streamlines in the reference experiment. Only a subsample of the velocity field is shown to avoid congestion of the figure. The largest velocity in the figure has an amplitude of 16.1 cm s^{-1} .

ciency and ϵ is the rate of TKE dissipation, one obtains

$$w_* N^2 = \frac{\partial}{\partial z}(k_\rho N^2) = \frac{\partial}{\partial z}(\Gamma \epsilon). \quad (10)$$

Assuming a uniform Γ value, as was done to estimate k_ρ from ϵ and N data (e.g., Polzin et al. 1997), the sign of w_* would be dictated only by the vertical gradient of turbulent dissipation. Mean ϵ profiles over the MAR in the Brazil Basin show a systematic increase with depth (e.g., St. Laurent et al. 2001), which would imply negative w_* . In contrast, ϵ profiles farther west off the MAR do not on average show systematic changes with depth (St. Laurent et al. 2001; their Fig. 2), which would imply much smaller w_* in absolute magnitude.

The negative w_* implied by ϵ data raises the question of the location of AABW upwelling required by the net AABW inflow at the basin boundaries (e.g., Polzin et al. 1997). These authors hypothesized that waters is fluxed strongly upward across density surfaces within the many canyons on the western flank of the MAR [Thurnherr and Speer (2003) estimated that the total length of connected “zonal” valley segments longer than 40 km below 1500 m and between 30°S and 2°N

associated with the ridge amounts to 47 000 km in the Brazil Basin]. On a broad scale, the fractured MAR would act as a “permeable sloping boundary,” with the densest waters of the basin entering at the western end of the canyons and exiting at the eastern end of the canyons (Polzin et al. 1997). Thus, the western flank of the MAR would actually be a site of AABW upwelling. St. Laurent et al. (2001) used an inverse model based on hydrographic and ϵ data to constrain the circulation near $\sim 21^\circ\text{--}22^\circ\text{S}$ on the western flank of the MAR. The inversion points to positive w_* on deep neutral density surfaces below the canyon crests and to negative w_* on shallower surfaces above the canyon crests west of the upwelling region. It revealed a zonal overturning circulation, which essentially supports the circulation hypothesized by Polzin et al. (1997). Morris et al. (2001) used the results of St. Laurent et al. (2001) to assume relatively large k_ρ near the axis of the MAR and smaller k_ρ west of the ridge in their analysis of the AABW mass budget in the Brazil Basin. Huang and Jin (2002) mentioned that bottom-intensified mixing in their PE model induces upwelling over the western slope of the MAR and downwelling over the lower part of the ridge and

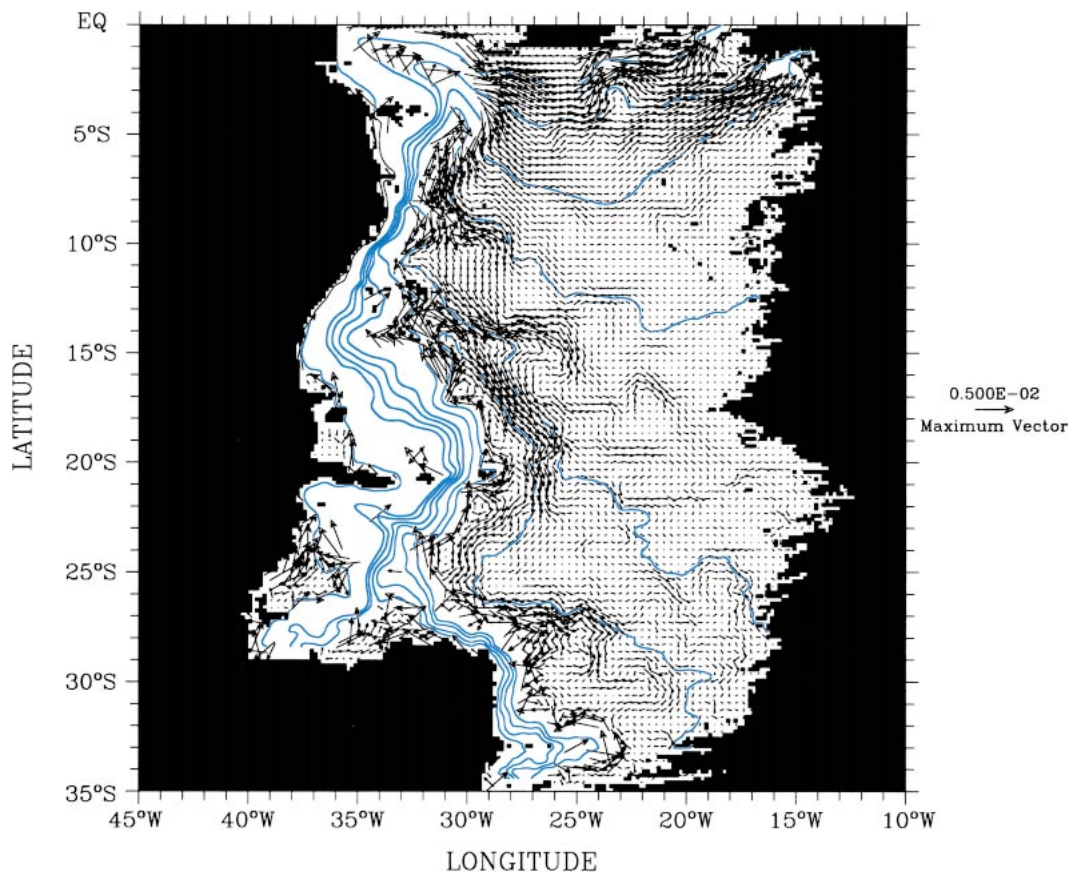


FIG. 6. Velocity field (m s^{-1}) and selected streamlines in the reference experiment (same streamlines as in Fig. 5). Only a subsample of the velocity field is shown to avoid congestion of the figure. The largest velocity in the figure has an amplitude of 5 mm s^{-1} in order to show the weak interior flow.

that this pattern is consistent with the results of St. Laurent et al. (2001).

We force the model with a highly idealized distribution of the cross-interface velocity $w(\mathbf{r})$. The distribution assumes a constant value of the velocity west (w_W) and east (w_E) of a critical longitude $\varphi_c(\vartheta)$ (ϑ being the latitude):

$$w(\varphi, \vartheta) = w_W \quad \text{if } \varphi \leq \varphi_c(\vartheta) \quad \text{and} \quad (11)$$

$$w(\varphi, \vartheta) = w_E \quad \text{if } \varphi > \varphi_c(\vartheta), \quad (12)$$

where $|w_W| \ll w_E$ and $w_E > 0$. Given the model resolution we do not attempt to account for the possible variability of $w(\mathbf{r})$ at spatial scales associated with the canyon-crest system in the western flank of the MAR, which has an estimated meridional wavelength of $\sim 30\text{--}60 \text{ km}$ (St. Laurent et al. 2001; Thurnherr and Speer 2003). However, the distribution defined by Eqs. (11)–(12) does capture essential features of the vertical circulation described by Polzin et al. (1997) and St. Laurent et al. (2001). That is, strong upwelling would occur near the MAR and small upwelling or downwelling would take place in the western interior far from the ridge. In practice, the field $w(\varphi, \vartheta)$ is calculated by

specifying the ratio $\lambda = w_W/w_E$ ($0 \leq |\lambda| \ll 1$) and using the integral constraint in Eq. (6). Therefore, each distribution $w(\mathbf{r})$ is dictated by two externally prescribed quantities: $\varphi_c(\vartheta)$ and λ . The first quantity determines the width of the region near the MAR where the net volume flux at the top of the AABW layer (3.7 Sv) takes place. The second governs the partitioning of this flux between this region and the western region.

We consider a first experiment with spatially variable w , using $\Delta\varphi_c = 4^\circ$ and $\lambda = 0$; that is, upwelling is confined to a region within 4° of the MAR and w vanishes elsewhere. The assumption that the upwelling region has a width of 4° on the western flank of the MAR is consistent with inverse model results (St. Laurent et al. 2001). The resulting flow in the region of the western boundary current differs little from the reference experiment (not shown). To elucidate the effects of a spatially variable $w(\mathbf{r})$ on the interior circulation, streamlines whose initial location approximately coincides with selected f/h_0 isopleths in the western part of the basin are again examined (red lines in Fig. 8). They differ strongly from the streamlines of the reference experiment. In the interior far from the ridge, the stream-

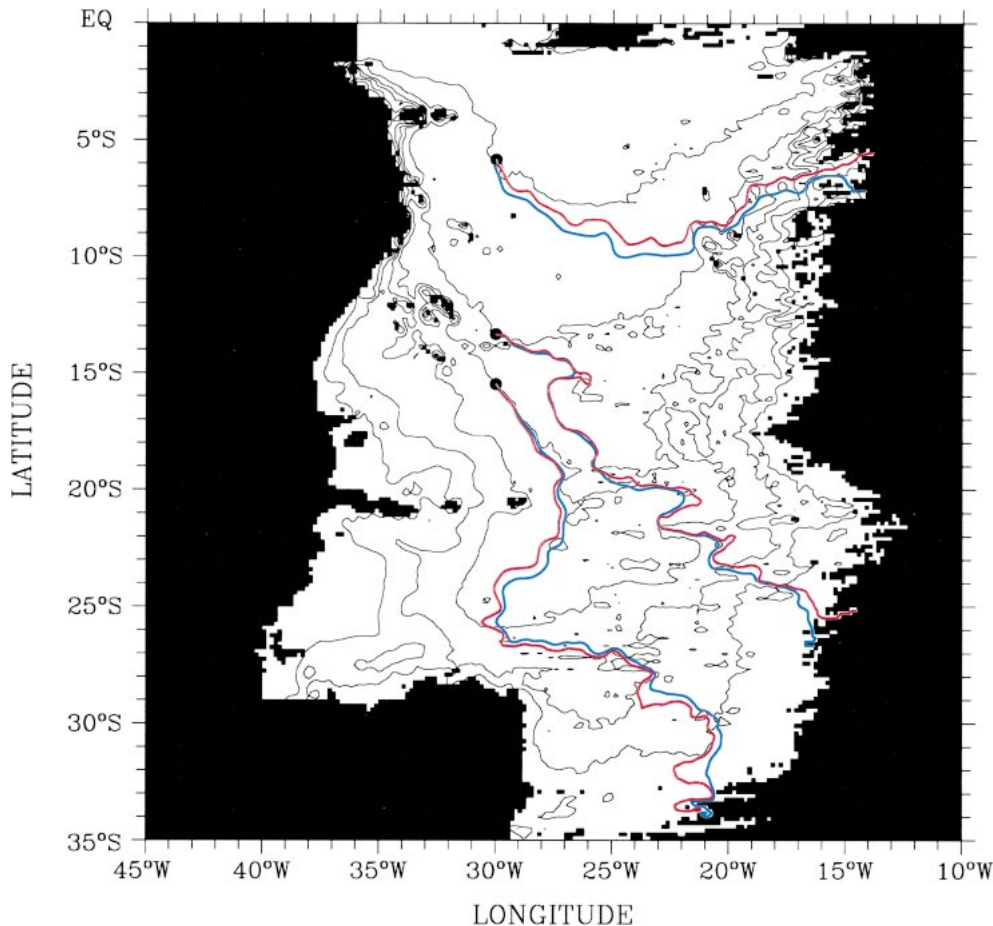


FIG. 7. Isopleths of potential vorticities f/h_0 (black) and simulated streamlines (blue and red). The simulated streamlines are for the reference experiment (blue) and another experiment similar to the reference experiment but with $A_v = 0.5 \times 10^{-2} \text{ m}^2 \text{ s}^{-1}$ and $A_h = 0.5 \times 10^3 \text{ m}^2 \text{ s}^{-1}$ (red). The initial location of each streamline (dots) is close to a f/h_0 contour.

lines tend to follow f/h_0 contours much more closely. Near the ridge they do intersect these contours, but the same is true for the streamlines of the reference experiment, as will be discussed in section 3d. The net result is that the southward component of the motion is on average reduced strongly by the confinement of the diapycnal mass flux near the ridge.

We examine a second experiment with $\Delta\varphi_c = 4^\circ$ as in the preceding experiment but with $\lambda = -0.1$; that is, small downwelling occurs west of the critical longitude $\varphi_c(\vartheta)$ (green lines in Fig. 8). This choice of $w(\mathbf{r})$ corresponds to a naive and qualitative extrapolation to the whole basin of inverse model results obtained for a region in the southeastern part of the basin (St. Laurent et al. 2001). In contrast to the previous experiment, some streamlines run north of their respective f/h_0 contours in the western interior. Additional experiments with $\Delta\varphi_c = 2^\circ$ or 6° indicate that the circulation responses to spatially variable $w(\mathbf{r})$ are insensitive to the width of the upwelling area (not shown).

d. Interpretation of numerical results

A simple interpretation of the model results is given, based on qualitative predictions from the linear PV balance (8) and idealized f/h_0 contours for the Brazil Basin (Fig. 9). The effect of frictional torque is neglected, and the western boundary region and the region influenced by the outflows at the Romanche–Chain FZs are excluded. The topographic and planetary β effects lead to a convergence of f/h_0 contours to the equator at both the western and eastern boundaries of the basin (if h_0 could vanish the contours would converge to a single point at both ends of the equator). The important dynamical consequence is the presence of (i) a positive zonal component of the linear PV gradient in the western part of the basin and (ii) a negative zonal component of the linear PV gradient in the eastern part. A barotropic flow that is purely geostrophic would be oriented northwest–southeast in the western part and southwest–northeast in the eastern part. The topographic and planetary

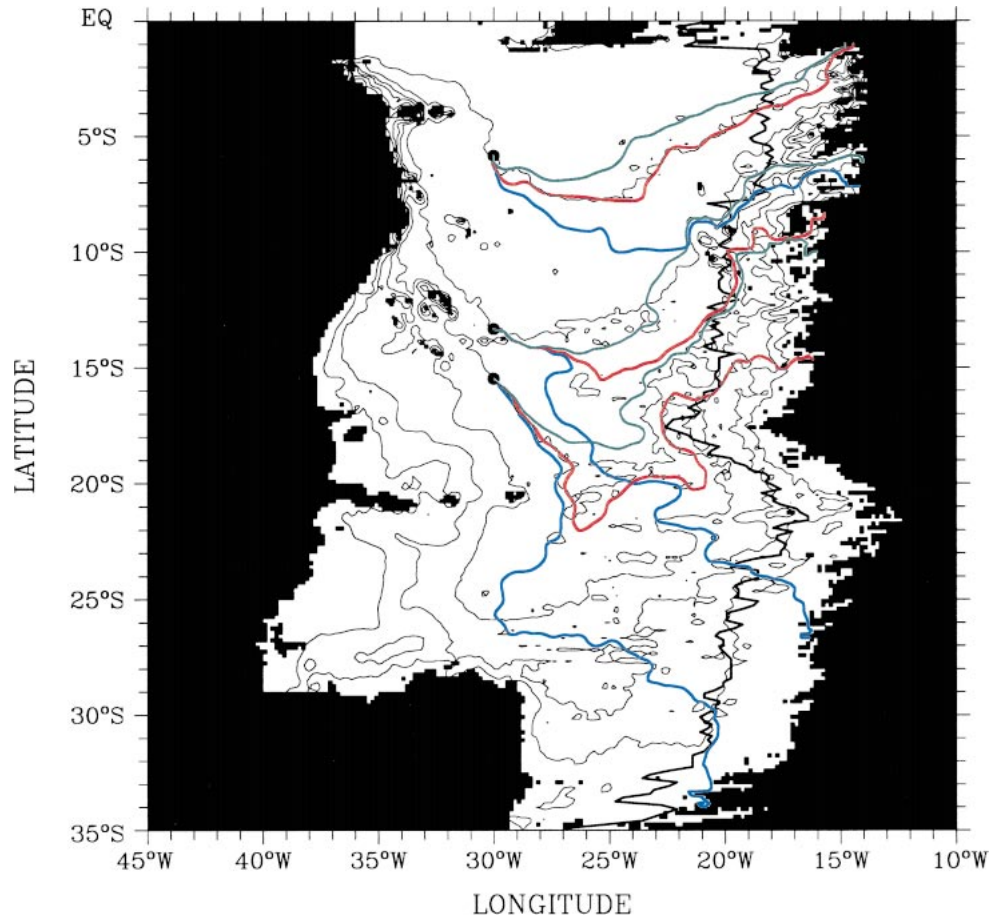


FIG. 8. Isopleths of potential vorticities f/h_0 (thin black lines) and streamlines in three different model experiments. The simulated streamlines are for the reference experiment (blue), a sensitivity experiment with $\Delta\varphi_c = 4^\circ$ and $\lambda = 0$ (red), and another sensitivity experiment with $\Delta\varphi_c = 4^\circ$ and $\lambda = -0.1$ (green). The initial location of each streamline (dots) is close to a f/h_0 contour. The critical longitude $\varphi_c(\theta)$ is also shown (thick black line).

β effects will compete with the net upwelling w , which tends to deflect the flow from f/h_0 contours.

In the constant- w case (line A in Fig. 9, and blue lines in Fig. 8), the vortex stretching ($wf/h_0 < 0$) displaces the streamlines to the right of the f/h_0 contours everywhere. In the variable- w case with $w_w = 0$ (line B in Fig. 9, and red lines in Fig. 8), the streamlines follow the f/h_0 contours until they get far into the eastern part of the basin. The stronger rightward displacement in the eastern part, with converging f/h_0 contours, does not compensate for the lack of rightward displacement in the region with diverging contours. The result is that the overall circulation is much more northward. In the variable- w case with $w_w < 0$ (line C in Fig. 9, and green lines in Fig. 8), the vortex compression in the western interior ($wf/h_0 > 0$) causes a leftward displacement and the overall circulation is even more northward.

Another feature of the simulations, which may at first seem surprising, is that the angle between the streamlines and the f/h_0 contours is much larger in the eastern part of the basin than in the western part, even in the

case with uniform upwelling. This means that the ratio between the velocity components parallel and perpendicular to the f/h_0 contours is smaller in the eastern part. The reason is that these components have rather different origin. The perpendicular component is driven by the local upwelling and does not vary systematically from west to east in the reference case (with constant w). The parallel component, on the other hand, is determined essentially by mass conservation, with the perpendicular component regarded as given. Thus, it is sensitive to the overall distribution of sources and sinks. In the present case the sources are in the western part of the basin, and if the sinks are distributed over the whole basin, mass conservation requires that the parallel component decreases from west to east. The same feature is present in the Stommel–Arons theory.

4. Comparison with previous studies

In this section we compare results from the shallow-water model with previous inferences about the circu-

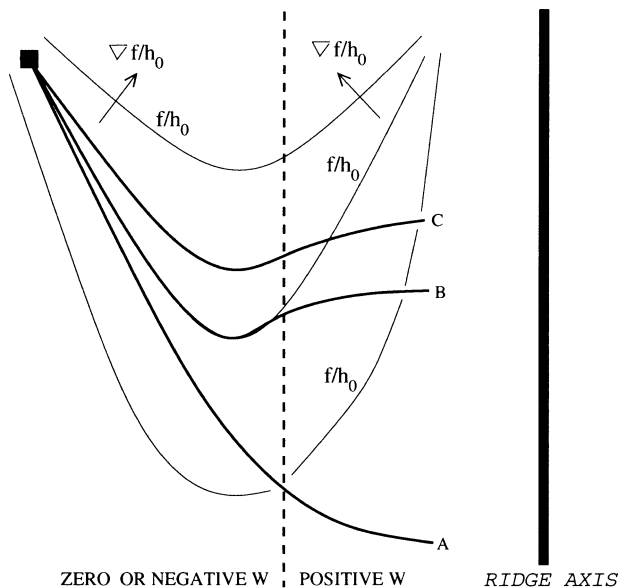


FIG. 9. Idealized potential vorticity f/h_0 contours and streamlines for the interior of the Brazil Basin. Streamline A corresponds to a spatially uniform cross-interface velocity w . Streamline B corresponds to a positive w in the region close to the ridge and to zero w west of that region. Streamline C corresponds to a positive w in the region close to the ridge and to negative w west of that region.

lation of AABW in the Brazil Basin. These inferences are based on hydrographic data, float trajectory data, and results from previous model studies.

a. Hydrographic data

It is noteworthy that estimates of geostrophic transport may vary between studies owing to a variety of reasons, such as real temporal variability, data quality and availability, bottom triangle approximation, and the choice of the level of no motion. Consider first some qualitative aspects of the circulation. Reid (1989) calculated adjusted steric heights at 4000 and 4500 dbar in the South Atlantic. His Figs. 29 and 30 include three isopleths in the Brazil Basin, which suggest the presence of a northward geostrophic flow throughout most of the basin south of $\sim 15^\circ\text{S}$. Our results with spatially uniform w are clearly not consistent with the existence of a northward flow in the interior of the basin (e.g., Fig. 5). Our results with spatially variable w are consistent with the existence of a northward flow in the eastern half of the basin away from the MAR but show a southward recirculation in the western half east of the western boundary current. Speer and Zenk (1993) inferred a southward flow of AABW in the western part of the basin (east of the DWBC) and a northward flow in the eastern part, by considering only the distribution of geostrophic contours. This circulation is different from the one predicted by the shallow-water model with uniform w but is essentially similar to the one predicted with spatially variable w . Note that it is the small value of w over most

of the basin assumed in the experiment with spatially variable w that makes this experiment agree with the flow scheme of Speer and Zenk (1993) (these authors ignored the effects of upwelling in their flow scheme). Demadron and Weatherly (1994) considered zonal and meridional hydrographic sections obtained for the South Atlantic Ventilation Experiment. They inferred the existence of three features: a southward return flow at the eastern edge of the DWBC, a northward flow in the eastern part of the basin (west of $\sim 20^\circ\text{W}$), and a cyclonic abyssal gyre in the central part of the basin north of $\sim 11^\circ\text{S}$. The first feature is present in all the numerical experiments considered above, whereas the second can be simulated only in experiments with variable w . None of our simulations, on the other hand, include a gyre in the northern central part of the basin.

A few quantitative estimates of geostrophic transport of AABW in the Brazil Basin have been published. McCartney and Curry (1993) examined two hydrographic sections near 23° and 11°S running across the entire basin. They estimated a net northward transport of 6.7 Sv at 23°S and 5.5 Sv at 11°S for AABW below a level of no motion located along the 1.9°C potential temperature isotherm. From sections spanning the whole zonal width of the basin, Speer and Zenk (1993) calculated a net northward transport of 5.0 ± 1.1 Sv at 24°S , 4.5 ± 0.8 Sv at 19°S , and 3.0 ± 1.4 Sv at 11°S , assuming a level of no motion along the $\sigma_t = 45.85 \text{ kg m}^{-3}$ surface. In the shallow-water model, the net northward transport amounts to 5.7–5.8 Sv at 23°S , 5.3–5.5 Sv at 19°S , and 4.4–4.5 Sv at 11°S , where the ranges reflect variations among the four experiments considered above. The zonally integrated transports predicted by the model appear comparable to the few observational estimates.

b. Float trajectories

We now attempt to compare model results directly with information provided by floats that were released at abyssal depths in the Brazil Basin (Hogg and Owens 1999). One important dynamical issue is whether the observed “zonality” in the trajectory of some of the floats released in the interior could be linked to the presence of enhanced diapycnal mixing near the MAR (Hogg and Owens 1999). The comparison is thus focused on the circulation in the interior, where horizontal variations in w were shown to have a substantial impact in the shallow-water model. We consider the floats that satisfy two criteria. First, we retain in the analysis only the floats that were launched at ~ 4000 m (in AABW) and that lasted at least 1 yr (Hogg and Owens 1999, their Fig. 6d). Second, we omit from the comparison the floats for which there is a clear visual indication of influences by the DWBC. A total of 18 floats satisfy these two criteria (Fig. 10).

We compare the AABW float trajectories with streamlines predicted by the shallow-water model in the experiment with spatially uniform w and in the experiment

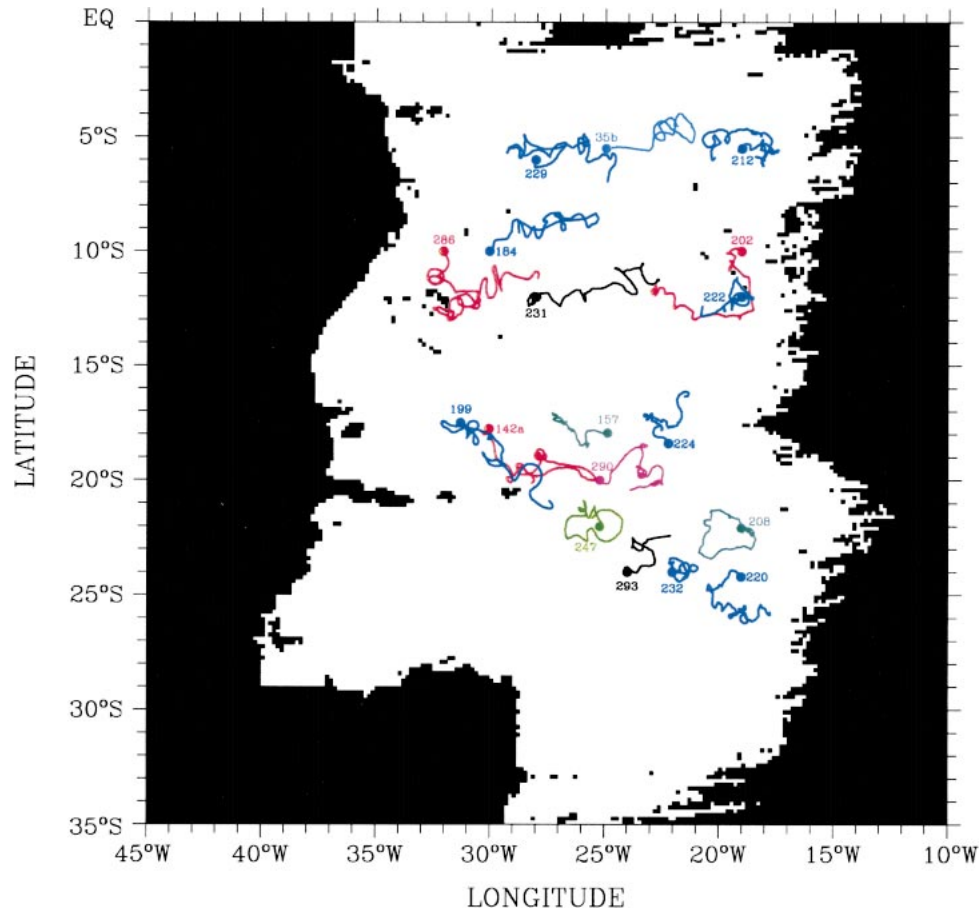


FIG. 10. Trajectory of 18 floats at abyssal depths in the Brazil Basin. Different colors are used to differentiate the individual float trajectories. Only the trajectories that were regarded as representative of AABW (Fig. 6d of Hogg and Owens 1999) and for which there is no clear visual indication of influences by the DWBC are shown. The numbers and dots denote the original float identification number and initial location, respectively (data from Hogg and Owens 1999). Isopleths of f/h_0 are also shown (black lines). The depths shallower than 3700 m are shaded.

with positive w near the MAR and zero w elsewhere (Fig. 11). Consider first whether the float trajectories and the model streamlines show (dis)similar flow directions. The float trajectories exhibit much more variations at small spatial scales than the model streamlines, which makes this qualitative comparison difficult. Nevertheless, it appears that the streamlines in both model experiments show important differences with float trajectories, although there are exceptions (e.g., 35b). The streamlines simulated with spatially variable w do not seem to compare more favorably to the float trajectories. The notable exception to this is for float 231, for which the prescription of a spatially variable w largely improves the fit of the model streamline to the float trajectory. At this point we do not have an explanation for why the fit is improved for this particular float.

We then compare the float data and the model results quantitatively. On each model streamline the geographic position after the time equal to the deployment period of the corresponding float is identified (pluses in Fig. 11).

For each streamline the distance to this position is much smaller than the distance between the initial and final locations of the corresponding float; that is, the velocities predicted by the shallow-water model are much smaller than the float velocities. We compute for each float the average float velocity over its trajectory:

$$\bar{u}_F = \int_{l_i}^{l_f} u_F dl / \int_{l_i}^{l_f} dl, \quad (13)$$

where l_i and l_f designate, respectively, the initial and final float location and u_F is the float velocity. The average float velocities \bar{u}_F are in the range 1.6–6.2 cm s^{-1} (Table 3 and circles connected by solid line in Fig. 12). The float velocities are compared with the shallow-water model velocities predicted in the four numerical experiments considered above with (i) spatially uniform w , (ii) spatially uniform w and reduced eddy viscosities, (iii) $w > 0$ near the MAR and $w = 0$ elsewhere, and (iv) $w > 0$ near the MAR and $w < 0$ elsewhere (Fig. 12). For a

consistent comparison we compute the line integral of the model velocity amplitude along each float trajectory:

$$\overline{|\mathbf{u}|} = \int_{l_i}^{l_f} |\mathbf{u}| dl / \int_{l_i}^{l_f} dl. \quad (14)$$

Note that the product $|\mathbf{u}| dl$ is used instead of $\mathbf{u} \cdot d\mathbf{l}$ as the integrand—that is we are interested in comparing the velocity amplitudes, not their projection, along the float trajectories. It appears that the model velocities are systematically lower than the float velocities, the difference reaching on average one order of magnitude (Fig. 12). Note also the large amplitude differences between experiments characterized by different $w_*(\mathbf{r})$. More specifically, the velocity amplitudes near the ridge (e.g., corresponding to the trajectory of floats 208, 222, and 224) are generally higher in experiments with variable w than in experiments with uniform w owing to the elevated vortex stretching near the ridge in the former experiments. Thus, the velocity amplitudes near the ridge simulated with variable w are closer to, but still substantially lower than, the float velocities.

It is also instructive to compare the float velocities with the velocity amplitudes predicted by the Stommel–Arons theory. An analytical expression for the velocity amplitude is derived from the theory

$$|\mathbf{u}_{\text{SA}}(\varphi, \vartheta)| = \frac{R}{h_0} w \sqrt{[2 \cos \vartheta (\varphi_E - \varphi)]^2 + \tan^2 \vartheta}, \quad (15)$$

where R is the earth radius and φ_E is the longitude of the eastern boundary of the basin. This expression is obtained by assuming a flat bottom, a constant pressure on the eastern boundary, a spatially uniform cross-interface velocity at the top of the layer (w), and an eastern boundary at a constant longitude (φ_E). To calculate $|\mathbf{u}_{\text{SA}}(\varphi, \vartheta)|$ we assume $h_0 = 1000$ m, $w = 5 \times 10^{-7}$ m s $^{-1}$, and $\varphi_E = 15^\circ\text{W}$. Like the line integrals of the model velocity amplitude, the line integrals of the theoretical velocity amplitude (circles connected by dashed line in Fig. 12) are much smaller than the float velocities. The theoretical and float velocities also differ by one order of magnitude on average.

c. Models

Our model results for the interior of the abyssal Brazil Basin show similarities but also differences with previous model studies. Spall (1994b) used a three-layer isopycnic PE model to study the effects of baroclinic instability of the western boundary current on the abyssal circulation in the interior. Whereas the model was not intended to simulate the circulation in a particular basin, the choice of the model basin (i.e., its idealized geometry and topography, and its location in the Southern Hemisphere) was motivated by observations in the Brazil Basin. The mass fluxes between the layers were assumed to be spatially uniform. When the western boundary current is

stable (as occurred in numerical experiments with a relatively high value for the bottom drag coefficient), these fluxes force a clockwise circulation gyre in the interior, modified by topography. This is qualitatively consistent with the Stommel–Arons theory and our shallow-water model. When it is unstable (with relatively small bottom drag), a mean circulation was found only in the statistical sense, characterized by anticlockwise motion in the interior. Stephens and Marshall (2000) used a model based on the shallow-water equations (neglecting local and advective accelerations in the momentum equation) to represent the flow of AABW in the entire Atlantic. All the simulations reported in their study assume a uniform w . The authors mentioned that the flows in their model occur predominantly along PV (f/h) contours, which is consistent with our results obtained for the region far from the ridge with spatially variable w . The results of Stephens and Marshall (2000), on the other hand, disagree with predictions by the Stommel–Arons theory and our numerical experiments with uniform w . In his two-layer, planetary geostrophic model forced by localized mixing over sloping bottom, Spall (2001) reported that the flow in the deep layer is very weak, zonal, and toward the east. This result is essentially similar with prediction by the present model.

The study of St. Laurent et al. (2001) provided important constraints on the circulation of AABW in a relatively small area of the Brazil Basin (between $\sim 25^\circ$ – 11°W and 25° – 19°S). The authors inferred, from an inverse model constrained by dissipation and hydrographic data collected in 1996–97, the flow in three layers corresponding to the neutral density ranges 28.08–28.16, 28.16–28.20, and >28.20 kg m $^{-3}$. They concluded that the flow in these layers is “generally southward and westward.” They demonstrated that their results are quantitatively consistent with tracer dispersion data for about the same region and period (Ledwell et al. 2000). Note that St. Laurent et al. (2001) mentioned that their estimated flow direction is not consistent with the adjusted steric heights calculated by Reid (1989), which suggest northward flow near 20°S , 20°W at 4000 (his Fig. 29) and 4500 dbar (his Fig. 30). Speer and Zenk (1993, their Fig. 13) and Demadron and Weatherly (1994, their Fig. 19) also inferred the presence of a northward flow of AABW in the region investigated by St. Laurent et al. (2001). The results from the shallow-water model obtained with spatially variable w show northeastward flow in the eastern half of the basin far from the MAR (Fig. 8). This is consistent with early inferences (Reid 1989; Speer and Zenk 1993; Demadron and Weatherly 1994) but disagrees with the more local estimates of St. Laurent et al. (2001).

5. Discussion

A first result of this study is the illustration of a strong sensitivity of bottom-water circulation to upwelling distribution in a shallow-water model with realistic topog-

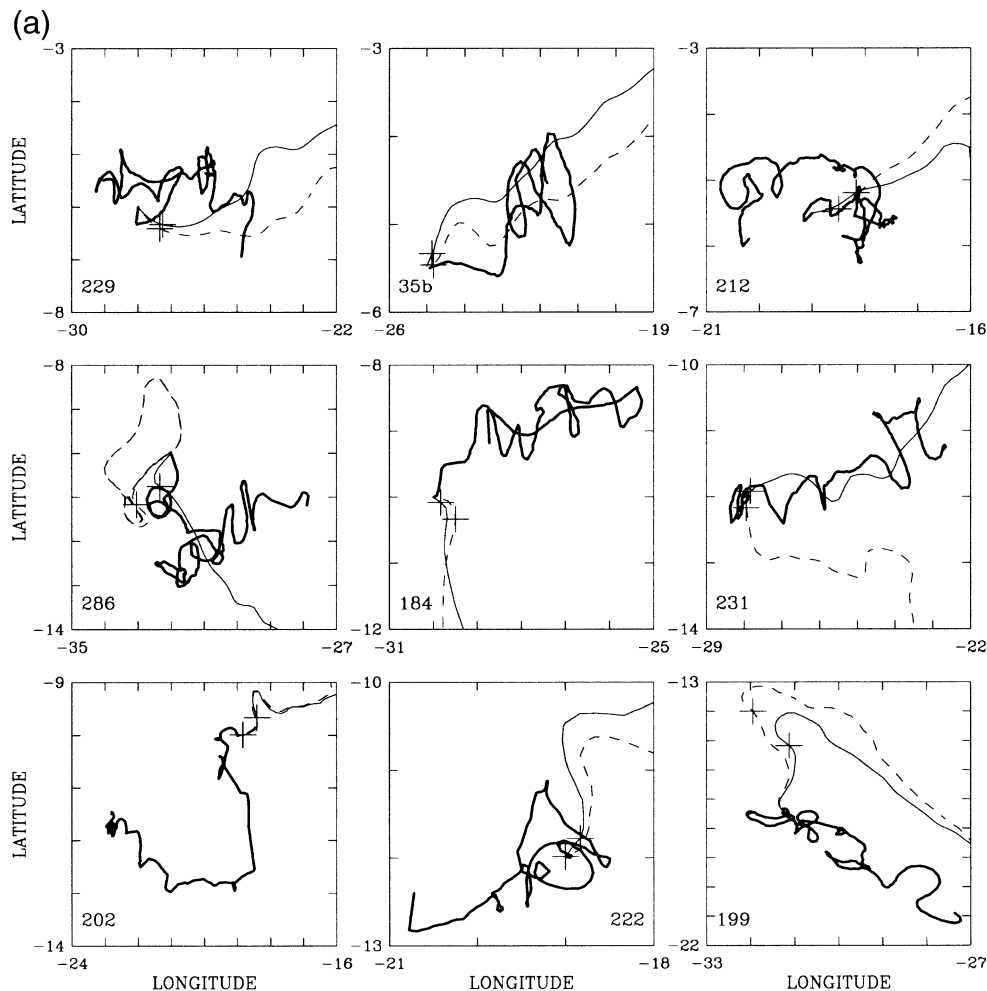


FIG. 11. Comparison between AABW float trajectories (thick solid line) and streamlines simulated by the shallow-water model in the experiment with spatially uniform w (dashed line) and in the experiment with a spatially variable w with $\Delta\varphi_c = 4^\circ$ and $\lambda = 0$ (thin solid line). The pluses on model streamlines indicate the position after a time equal to the deployment period of the corresponding float. The number in each panel is the float identification number (ID).

raphy. If the upwelling is confined to the region of rough topography near the model ridge, as suggested by dissipation data for the Brazil Basin, the poleward motion as predicted by the Stommel–Arons theory is strongly reduced, or even reversed. This result arises in the shallow-water model mostly from the combination between two effects: (i) the net gradient of ambient potential vorticity set by the topography and the variation of the Coriolis parameter with latitude, and (ii) the spatial distribution of the PV flux at the top of the abyssal layer. The first effect tends to align barotropic motion with f/h_0 contours, which in the Brazil Basin diverge to the southeast in the western part of the basin and converge to the northeast in the eastern part. The second tends to deflect barotropic motion to the right of f/h_0 contours in the Southern Hemisphere. The first effect essentially dominates in the western interior, where net upwelling is low, whereas the second becomes very important

close to the ridge, where upwelling is high. If the upwelling is limited to a small region close to the ridge, the motion is equatorward just west of this region and quasi zonal within this region. This largely reduces the zonally integrated transport to the south in the interior. For example, the zonally integrated transport east of 30°W is southward at 23°S (11°S) in the two experiments with uniform w , amounting to -0.77 Sv (-0.59 Sv) in the reference experiment and to -0.71 Sv (-0.59 Sv) in the experiment with reduced viscosities. By contrast, this transport at 23°S (11°S) is northward in the two experiments with spatially variable w , reaching 0.39 Sv (0.45 Sv) in the experiment with $w = 0$ far from the ridge and 1.57 Sv (1.54 Sv) in the experiment with $w < 0$ far from the ridge. The differences in the transport rates between the experiments with uniform and variable w are on the same order of magnitude as the estimated net inflow of 3.7 Sv into the basin (Table 1). This il-

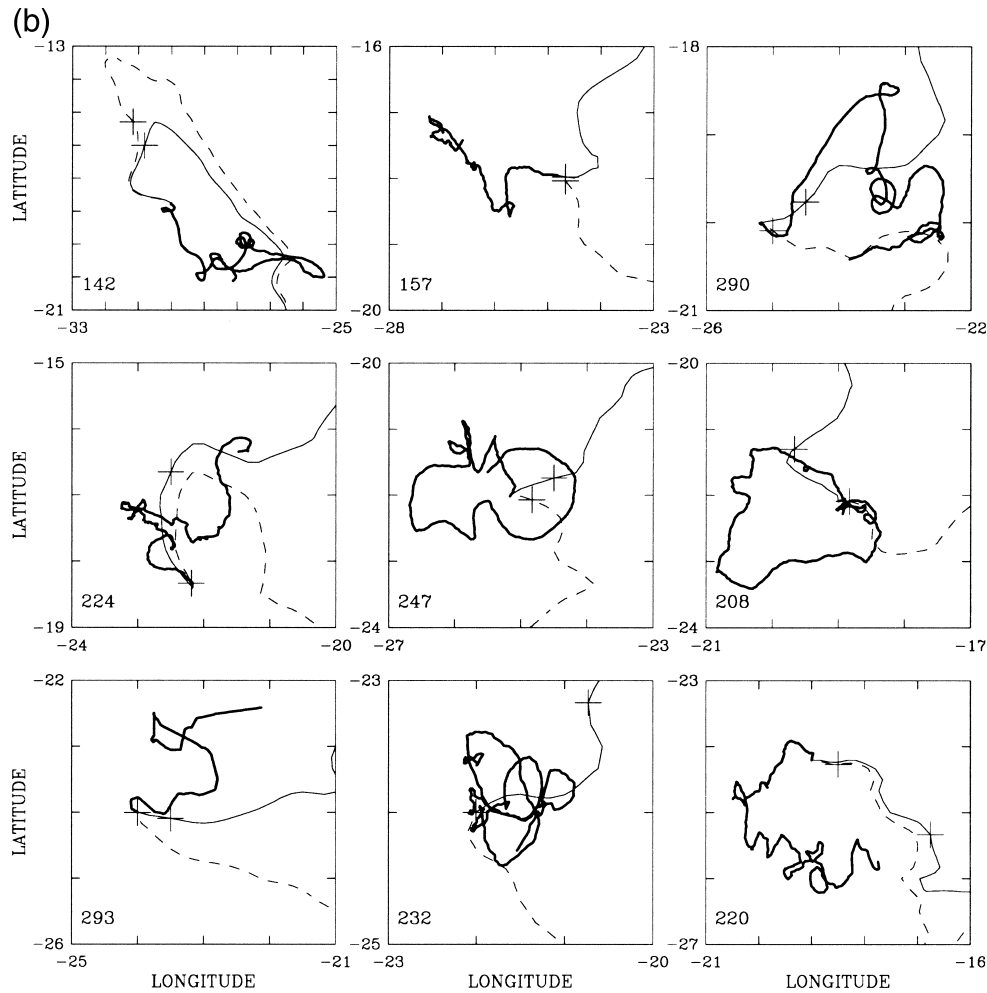


FIG. 11. (Continued)

illustrates the strong influence of $w(\mathbf{r})$ on the interior circulation.

A second result of our study is the important differences between the predictions of the shallow-water model and the float data for AABW in the Brazil Basin. The model streamlines and velocities show important differences with the float trajectories and velocities. These differences are obviously the result of missing physics in the model. To better identify the missing physics we first consider more closely the trajectories of the floats launched in the AABW layer during the DBE (Hogg and Owens 1999). The trajectories seem actually to reveal an important influence by an abyssal eddy field (Fig. 10). Data from current meters deployed at ~ 2500 m during the DBE indicated TKE levels of order $1 \text{ cm}^2 \text{ s}^{-2}$ in the basin interior (Hogg and Owens 1999). Despite these low levels, as noticed by these authors, a surprising number of floats were caught in vortices. Evidence of abyssal eddies in the Brazil Basin was also found from hydrographic casts (Weatherly et al. 2002). It is noteworthy that zonal motion is suggested

by many, but not all, float trajectories (Fig. 10). Among the floats that experienced approximately zonal trajectories, many showed back-and-forth motions. LaCasce (2000) conducted a statistical analysis of the trajectory of the floats released at the NADW and AABW levels during the DBE. He concluded that the floats in the interior show no significant drift in any direction, despite that some floats move only westward and others only eastward during their deployment period. It is instructive to compare for each float the net displacement between its initial and final locations with the total distance traveled by the float during its whole deployment period. Floats 142a, 184, 212, 229, 286, and 35b have a ratio of total distance to net displacement equal to, respectively, 5.6, 10, 13, 5.7, 5.6, and 3.4 (Table 3). For these floats the period of the zonal oscillations is comparable to the deployment period (Table 3). The AABW floats present other puzzles (Hogg and Owens 1999). For example, all floats launched in the northern half of the basin and along its eastern edge near 19°W experienced a net displacement to the west (Hogg and Owens

TABLE 3. Trajectory statistics for floats released in the AABW of the Brazil Basin.

Float ID	T^a (day)	L^b (km)	$\int_{l_i}^{l_f} dl^c$ (km)	$\int_{l_i}^{l_f} dl/L$	$\int_{l_i}^{l_f} u_F dl / \int_{l_i}^{l_f} dl$ (cm s ⁻¹)
142a	621	328	1829	5.6	4.6
157	821	198	724	3.7	1.6
184	793	166	1656	10	3.0
199	783	556	2069	3.7	4.3
202	791	448	1459	3.3	3.0
208	791	023	1117	49	2.2
212	793	139	1750	13	3.7
220	793	213	1237	5.8	2.6
222	510	193	1054	5.5	3.7
224	793	240	953	4.0	2.1
229	793	361	2069	5.7	4.1
231	795	580	1479	2.6	3.1
232	793	057	973	17	2.0
247	793	053	1214	23	2.5
286	793	468	2626	5.6	6.2
290	793	146	1252	8.6	2.7
293	595	260	636	2.5	1.6
35b	444	361	1235	3.4	4.3

^a Approximate length of time between initial and final locations of the float.

^b Geodesic distance between initial and final locations of the float.

^c Total distance traveled by the float between its initial and final locations.

1999, their Fig. 6c). There also appears a collision course with two floats (202 and 231) deployed in the middle of the basin (Hogg and Owens 1999, their Fig. 8a). These authors argued that some of the float “mysterries” will be solved through a more extensive float dataset and by taking temporal variability into account.

In the remainder of this section we discuss some mechanisms that are not represented in our numerical experiments but which may have influenced strongly the floats released in the AABW layer of the Brazil Basin. The differences between the float data and the results from our numerical experiments may be largely associated with their lack of any time-dependent motion. The float velocities (Table 3, Fig. 12) have an order of magnitude comparable to the rms velocities from current meters deployed at ~ 2500 m in the basin, which were interpreted in terms of eddy activity (Hogg and Owens 1999). The discussion below is largely devoted to mechanisms that may be responsible for the presence of zonal motions and/or eddies in the abyssal interior.

a. Geostrophic turbulence

Zonal motions in the subthermocline region can be produced by the elongation of an abyssal eddy field in the zonal direction owing to the planetary β effect. LaCasce and Speer (1999) used a quasigeostrophic (QG) model to simulate particle trajectories in a turbulent unforced barotropic flow on the β plane. In the simulation, most trajectories show a systematic zonal drift, the direction of the drift depending on the initial position,

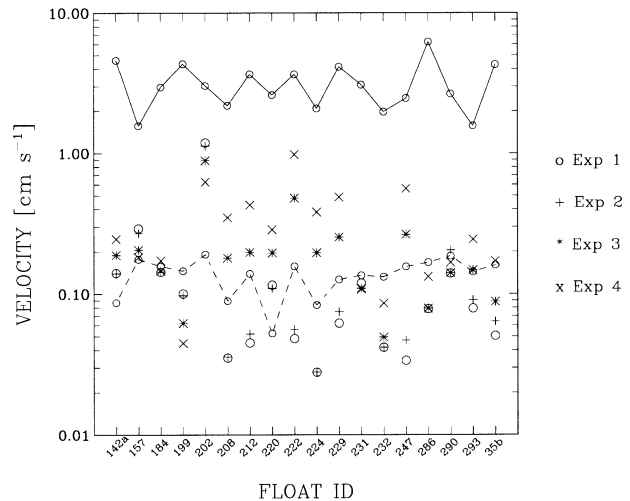


FIG. 12. Velocity amplitudes estimated from the floats released in the AABW in the Brazil Basin (circles connected by solid line), calculated from the Stommel-Arons theory (circles connected by dashed line), and simulated in the four numerical experiments considered in this study (other symbols). Experiment 1 is the reference experiment but with the values of A_e and A_s reduced by a factor of 2. Experiment 3 corresponds to a spatially variable w with $\Delta\varphi_c = 4^\circ$ and $\lambda = 0$. Experiment 4 corresponds to a spatially variable w with $\Delta\varphi_c = 4^\circ$ and $\lambda = -0.1$. The numbers below the horizontal axis are the float identification numbers. Only the floats for which the trajectories were regarded as representative of AABW (Fig. 6d of Hogg and Owens 1999) and for which there is no visual indication of influences by the DWBC are considered (data from Hogg and Owens 1999). Note the logarithmic scale.

with some particles moving west and others east. The simulated trajectories (Fig. 3 of LaCasce and Speer 1999) do not look unlike some of the AABW trajectories in the interior of the Brazil Basin (Fig. 10). A quantitative assessment of the importance of this mechanism may be attempted. According to the QG approximation, the conversion of eddies into Rossby wave packets leads to a statistically stable peak in the energy spectrum at wavenumber $\sqrt{\beta/U}$, where U is a typical velocity amplitude of the eddy field (Pedlosky 1987). The Rhines scale $\sqrt{U/\beta}$ provides a measure of the meridional scale of the zonal jets. Assuming that the rms velocities of $O(1 \text{ cm s}^{-1})$ measured by current meters at ~ 2500 m in the basin (Hogg and Owens 1999) are also representative of levels in the AABW, this scale amounts to ~ 20 km at the midlatitude of the basin. This is smaller than the meridional scale that is apparent in individual float trajectories (e.g., floats 229, 35b, 212, 184, and 231; Fig. 11). The assessment is very crude and at best suggests that more energetic conditions may be required for geostrophic turbulence to be a dominant mechanism affecting the AABW floats.

b. Fractured ridge

Zonal jets may occur on the western side of a basin possessing a meridional ridge pierced by gaps (e.g., Ped-

losky 1994). Pedlosky (2001) applied a two-layer QG model to a basin including a meridional fractured ridge, to suggest that the zonal jets might explain float data at about 22°S examined by Hogg and Owens (1999). Mercier et al. (2000) inferred from a meridional hydrographic section along the eastern flank of the MAR, that “bottom water” throughflows occur at the Rio de Janeiro FZ (22°S) and Rio Grande FZ (26°S). The water fluxes, however, have not been quantified and their significance for the mass budget of AABW in the Brazil Basin is unknown (accordingly only AABW fluxes through the Romanche–Chain FZs have been considered in the shallow-water model). On the other hand, the AABW float trajectories that show best visual evidence for zonal motions actually occur north of 22°S (Fig. 10). It seems a priori likely that the outflows at the Romanche–Chain FZs (Mercier and Speer 1998) did influence some float trajectories. In the shallow-water model the circulation in the northern part of the basin is strongly influenced by the presence of these FZs, where mass fluxes are specified; this is apparent both in the experiment with uniform w (Fig. 6) and in the experiment with variable w (Fig. 8). On the other hand, the floats that experienced quasi-zonal trajectories, namely, those in the northernmost part of the basin, did not move in one particular direction but tended to oscillate (floats 229, 35b, 212, 184; Figs. 10 and 11). Thus, there appears to be no strong support in favor of the role of gaps in the MAR on the AABW float trajectories, at least not in the way envisioned by the aforementioned theories.

c. Eddies produced by surface wind

The possible importance of eddies for the abyssal circulation has long been established. For example, Holland and Lin (1975) used a two-layer PE model with relatively small viscosity and high spatial resolution to simulate the circulation driven by steady wind in a single-gyre basin. In this model the eddies which can appear spontaneously as a result of baroclinic instability are uniquely responsible for the establishment of a mean circulation in the lower (abyssal) layer, with velocities of $\sim 1 \text{ cm s}^{-1}$. Important is that the establishment of the mean circulation in the deep layer proceeds through pressure forces acting at the interface between the two layers, a forcing not represented in the shallow-water model. Holland (1978) applied a two-layer QG model driven by steady wind to single- and double-gyre basins. They show that eddies generated by instabilities of the surface flow create a downward momentum flux that fills the lower (abyssal) layer with eddy energy and produces there time-mean gyres. The downward transfer of kinetic energy proceeds again through inviscid pressure forcing at the interface, generating abyssal velocities as large as $O(10) \text{ cm s}^{-1}$ in some experiments. Holland and Rhines (1980) examined in detail one particular numerical experiment of Holland (1978), which was regarded as having the most “realistic” behavior.

In this experiment the deep ocean contains eddy energy far in excess from the mean. The pressure forcing at the interface is accompanied by downgradient PV flux everywhere in the lower layer. These authors hence postulated that the deep dynamics is characterized by a “turbulent” Sverdrup balance:

$$\bar{\mathbf{u}} \cdot \nabla \bar{Q} = \nabla \cdot (-\overline{\mathbf{u}'Q'}), \quad (16)$$

where \mathbf{u} is here the three-dimensional velocity vector, Q is the potential vorticity in the QG approximation, $(\bar{\quad})$ is a mean value, and $(\quad)'$ is a perturbation. The balance indicates that the mean flow would be determined by the divergence of the eddy PV flux and by the mean PV gradient. In particular, the vertical forcing on the abyssal circulation would arise from the correlations between the fluctuations of vertical velocity and PV. This differs fundamentally from the view, explicit in the Stommel–Arons theory and the shallow-water model, that the abyssal flows are driven by a vertical velocity w unrelated to the deep dynamics.

d. Density stratification and baroclinic instability

The absence of density stratification is a major physical deficiency of the shallow-water model (Pedlosky 1987) and its importance in the misfit between the float data and the model must also be discussed. It is instructive in this regard to examine the AABW float trajectories in the longitude–pressure plane (Fig. 13). Several floats sank by several hundred decibars during their deployment period, owing presumably to a decrease of float buoyancy through time (N. Hogg 2003, personal communication). It could be speculated that the changes in float direction with depth reflect, at least partly, the presence of baroclinic motions within the AABW layer.

According to continuously stratified models, two possible causes of strong baroclinic velocities as compared with the average velocities over the whole abyssal layer in the interior are longitudinal variations in diapycnal advection (Pedlosky 1992) and a vertical shear in the mass fluxes at the basin boundaries (Edwards and Pedlosky 1995). Observations for the Brazil Basin are consistent both with important longitudinal variations in diapycnal mixing (Polzin et al. 1997; Ledwell et al. 2000; St. Laurent et al. 2001) and with substantial vertical shear in the AABW fluxes at the rims of the basin (Mercier and Speer 1998; Hogg et al. 1999; Zenk et al. 1999).

Spall (1994b) noted that the sum of the two bottom-most layers in his three-layer isopycnic model approximately represents the AABW in the Brazil Basin. He illustrated that the baroclinic instability of the DWBC over the sloping bottom can drive the interior circulation through lateral PV stresses [Eq. (16)]. This contrasts with previous works that pointed to a source of eddy variability outside the abyssal layers and to the role of vertical stresses (e.g., Holland 1978; Holland and Rhines 1980). Spall (1994b) showed that, in an experiment with unstable DWBC, the eddy variability is dominated by

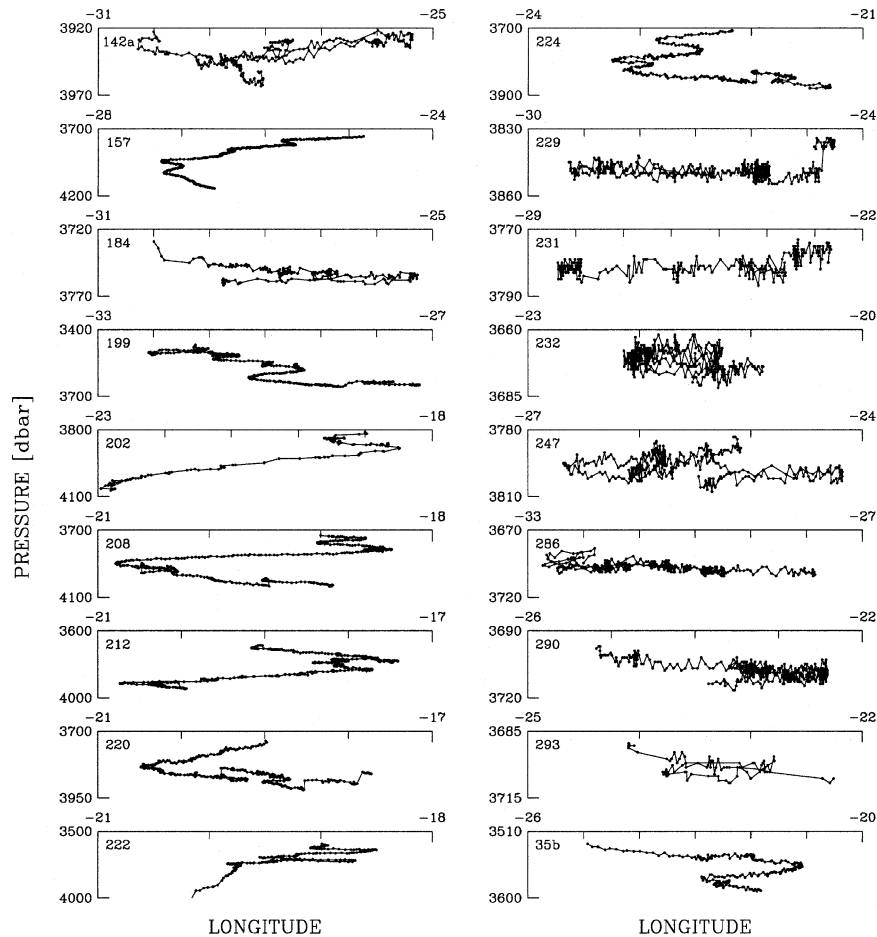


FIG. 13. Trajectory of 18 floats in the AABW of the Brazil Basin in the pressure–longitude plane. Each trajectory is entirely confined in the corresponding panel except for float 222 (bottommost left panel) whose latest recorded pressure is 4762 dbar. The pressure and longitude scales are different in each panel (data from Hogg and Owens 1999).

two frequencies, corresponding to periods of about one month and one year, and that the eddy fluxes are carried by topographic waves with a velocity amplitude estimated to $O(1)$ cm s^{-1} . The longest period is not inconsistent with the period of the zonal oscillations observed for some AABW floats (Fig. 10; Table 3), whereas the wave velocity amplitude has an order of magnitude comparable to that of the velocities measured by current meters at ~ 2500 m (Hogg and Owens 1999) and of the float velocities (Fig. 12).

Another possible mechanism is the baroclinic instability of a mean meridional flow (Spall 1994a). Treguier et al. (2003) calculated unstable modes of the mean meridional flow and found them to be of the scale of the zonal currents observed in the Brazil Basin. They concluded that the role of these unstable modes does not seem to be important in their models but that they may become more so at higher resolution. Thus, baroclinic instabilities appear as possible mechanisms to accelerate the interior flow, although their importance for the lagrangian transport in the interior of the Brazil Ba-

sin as revealed by AABW floats would require a specific investigation.

e. Rossby waves

Other mechanisms may also generate low-frequency zonal motions in the subthermocline region. The simplest mechanism is probably the propagation of a single Rossby wave of finite amplitude. LaCasce and Speer (1999) used the QG model for a barotropic fluid to simulate numerically the trajectory of particles advected by a single Rossby wave in a channel bounded meridionally. The simulated drift velocity is either eastward or westward, despite the fact that the wave speed is uniquely westward, and varies in both horizontal directions. This pattern is not inconsistent with some float trajectories for the AABW layer (Fig. 10).

Rossby waves generated by surface wind have been proposed as a primary mechanism of zonal flows in the subthermocline region (Nakano and Sugihara 2002; Treguier et al. 2003). Treguier et al. (2003) compared

the trajectories simulated by two different z -coordinate PE models with the trajectories of floats deployed at ~ 2500 m in the Brazil Basin (Hogg and Owens 1999). The authors did not consider the deeper level of the AABW, where none of the models was deemed to be very realistic. Comparison of model results with results from an idealized tropical Atlantic model that is almost entirely wind-driven, gave evidence that the zonal flows in the PE models, which resemble the float trajectories within the NADW, arise from wind forcing. It seems conceivable that wind forcing importantly affected the trajectories of the AABW floats as well. On the other hand, the model simulations examined by Treguier et al. (2003) do not consider the presence of enhanced diapycnal mixing near the MAR (e.g., Polzin et al. 1997; Ledwell et al. 2000; St. Laurent et al. 2001). Huang and Jin (2002) showed that a simple representation of bottom-intensified diapycnal mixing near the ridge has a profound influence on the abyssal circulation in a z -coordinate PE model of the South Atlantic. When bottom-intensified mixing is included, the simulated circulation in the Brazil Basin is dominated by meridional rather than zonal motions. More specifically, it is characterized by (i) a strong bottom current along the western slope of the MAR (at depth > 3 km), which is almost as strong as the DWBC, and (ii) a flow on the seafloor that is generally equatorward (Huang and Jin 2002, their Fig. 1).

Inspection of the AABW float trajectories shows that zonal motions are mostly apparent near the equator (Fig. 10). It appears well established that variability in the deep equatorial ocean can partly be described in terms of linear waves forced by surface winds (Thierry et al. 2004, and references therein). In particular, these authors provided evidence that the deep seasonal variability in PE models of the equatorial Atlantic Ocean is mainly forced by the zonal wind fluctuations in the equatorial band. According to Thierry et al. (2004) wind energy in the investigated model simulations reaches the deep layers via vertically propagating Kelvin and Rossby waves, with Rossby waves with high meridional modes ($l > 1$) contributing to the deep seasonal variations. Future work is necessary to explore the possibility that wind forcing was an important mechanism affecting the float trajectories in the AABW layer.

6. Conclusions

In this work a numerical model based on the shallow-water equations is developed in an attempt to address some important issues about the abyssal circulation raised by data from the Deep Basin Experiment in the Brazil Basin. We formally address the problem of the circulation of a rotating, incompressible, and homogeneous fluid (representing the AABW) subject to a horizontally varying mass flux at its free surface and resting on a variable bathymetry (Brazil Basin). In the model layer the relative vorticity is small compared to the planetary vorticity,

except in the western boundary current where most of the kinetic energy is concentrated. To characterize and interpret dynamically the numerical flows, model streamlines are compared to contours of linear potential vorticity of the shallow-water theory. We find that the Stommel–Arons, poleward motion in the interior can largely be reduced, or even reversed in sign, if the upwelling is confined to the proximity of the ridge. This result is interpreted in terms of a balance between the topographic and planetary β effects and the distribution of vortex stretching at the top of the layer. It suggests the need for an accurate representation of diapycnal mass fluxes in shallow-water models and isopycnal models aimed at a realistic simulation of abyssal circulations.

The shallow-water model can produce results that are consistent with some (but not all) estimates of AABW transport patterns and rates in the basin based on hydrographic data. On the other hand, the model streamlines and velocities show important differences with the trajectory and velocity of the floats launched in the AABW. The float data provide a picture of the abyssal circulation that is much more energetic and variable than the one envisioned by the Stommel–Arons theory (a steady-state theory) and the shallow-water model, at least as it is formulated and numerically solved in this study. The Eulerian velocities in our numerical experiments are on average an order of magnitude smaller than the float velocities and constant in time. The prescription of very small net upwelling in the interior far from the ridge does not systematically improve the fit of the model streamlines to the float trajectories. Thus, our experiments do not support the hypothesis that zonal motions, which are apparent in some float trajectories, result from vanishing buoyancy forcing in the interior (Hogg and Owens 1999).

The differences between the float data and the model results give some insight into the dynamical interpretation of the float data and into the limitations of the model. A variety of mechanisms (in addition to spatial variations in buoyancy forcing), which are absent from our experiments, may have strongly influenced the AABW floats. From simulations with PE models wind forcing was proposed as a primary mechanism for the zonal trajectories of floats released in the NADW (Treguier et al. 2003). However, not all floats in the underlying AABW show zonal motions and it is not clear whether model trajectories in the deeper AABW are robust against the assumed distribution of vertical (or diapycnal) mixing (Huang and Jin 2002). Other plausible mechanisms that may have strongly influenced the AABW floats are quite varied, including β turbulence, density stratification and the baroclinic instabilities of DWBCs and meridional flows, and the advection by Rossby waves.

Our study highlights the limitations of the shallow-water model to produce realistic simulations of ocean abyssal flows, at least as they are pictured by observations from neutrally buoyant floats. Thus, our results should be regarded more as conceptual experiments

rather than a more realistic simulation of the AABW in the Brazil Basin in comparison with previous model studies. The limited capability of our experiments to replicate the float data may be largely associated with the omission of potentially important dynamical interactions with the layers overlying the AABW in the Brazil Basin. This is a major drawback of the shallow-water model, for which these interactions are limited to the prescription of interfacial mass fluxes. Moreover, as shown in previous studies (e.g., Kawase 1987) and here, the parameterization of these fluxes is critical in determining the flow in the model.

Acknowledgments. We thank Karl Helfrich for helpful discussions about the numerical solution of the shallow-water equations. Discussions with Michael McCartney and Nelson Hogg about the circulation of AABW in the Atlantic and float data of the DBE are gratefully acknowledged. Comments from three reviewers allowed us to improve significantly both the content and the presentation of the manuscript. The very detailed comments of one reviewer in particular were deeply appreciated. We also benefited from interesting discussions with Gregg Holloway and Ann Gargett about diapycnal mixing in the deep ocean. Louis St. Laurent kindly sent us bathymetric roughness data. OM acknowledges the support from the Penzance Endowed Fund in Support of Assistant Scientists.

APPENDIX

Calculation of Streamlines

Consider a water particle located on the meridional boundary of a model grid cell with the zonal velocities $u_{i,j-1/2}$ and $u_{i+1,j-1/2}$ defined at its meridional boundaries and the meridional velocities $v_{i+1/2,j-1}$ and $v_{i+1/2,j}$ at its zonal boundaries (open circle in Fig. 3). Within the cell u is assumed to be a linear function of longitude φ only and is calculated from the boundary values $u_{i,j-1/2}$ and $u_{i+1,j-1/2}$. Similarly, v is assumed to be a linear function of latitude ϑ only and is computed from $v_{i+1/2,j-1}$ and $v_{i+1/2,j}$. The streamline within the cell is then the set of points satisfying two ordinary differential equations:

$$R \cos \vartheta_p \frac{d\varphi_p}{dt} + \varphi_p \alpha_1 + \alpha_2 = 0 \quad \text{and}$$

$$R \frac{d\vartheta_p}{dt} + \vartheta_p \gamma_1 + \gamma_2 = 0,$$

where φ_p and ϑ_p are the longitude and latitude of the particle, respectively, R is the earth radius, and

$$\alpha_1 = \frac{u_{i,j-1/2} - u_{i+1,j-1/2}}{\Delta \varphi},$$

$$\alpha_2 = \frac{\varphi_i}{\Delta \varphi} (u_{i+1,j-1/2} - u_{i,j-1/2}) - u_{i,j-1/2},$$

$$\gamma_1 = \frac{v_{i+1/2,j-1} - v_{i+1/2,j}}{\Delta \vartheta}, \quad \text{and}$$

$$\gamma_2 = \frac{\vartheta_{j-1}}{\Delta \vartheta} (v_{i+1/2,j} - v_{i+1/2,j-1}) - v_{i+1/2,j-1}.$$

The two ordinary differential equations (ODEs) above are coupled by the function $\vartheta_p(t)$. The zero- and first-order terms in the Taylor expansion $\cos(\vartheta_0 + \Delta \vartheta) = \cos \vartheta_0 (1 - \tan \vartheta_0 \Delta \vartheta) + O[(\Delta \vartheta)^2]$ differ by less than 0.002 $\cos \vartheta_0$ in absolute magnitude for $-35^\circ < \vartheta_0 < 0^\circ$ and $\Delta \vartheta = 10'$. Taking $d \cos \vartheta_p / dt = 0$ in the first ODE is thus a very good approximation to describe the zonal motion of the particle in the cell. The two ODEs can then be individually integrated analytically, yielding the solutions $\varphi_p = \varphi_p(t)$ and $\vartheta_p = \vartheta_p(t)$. In practice these solutions are used to calculate the time it takes for the particle to reach the different boundaries of the cell. Consider the case $u_{i,j-1/2} > 0$ so that the particle moves eastward. The time necessary to reach the eastern boundary amounts to

$$t_E = \frac{R \cos \vartheta_p}{\alpha_1} \ln \left(\frac{\varphi_i + \alpha_2 / \alpha_1}{\varphi_{i+1} + \alpha_2 / \alpha_1} \right).$$

Similar expressions can be found for the time necessary to reach the northern (t_N) and southern boundary of the cell (t_S). The actual path of the particle is then given by the minimum of t_E , t_N , and t_S . One particular but possible situation occurs when the flow field is locally convergent, that is, $u_{i,j-1/2} > 0$, $v_{i+1/2,j} < 0$, $u_{i+1,j-1/2} < 0$, and $v_{i+1/2,j-1} > 0$. When this occurs the particle is virtually lost from the domain and the calculation of the streamline is stopped.

REFERENCES

- Arakawa, A., and V. R. Lamb, 1981: A potential enstrophy and energy conserving scheme for the shallow water equations. *Mon. Wea. Rev.*, **109**, 18–36.
- Bretherton, F. B., and D. Haidvogel, 1976: Two-dimensional turbulence over topography. *J. Fluid Mech.*, **78**, 129–154.
- Crease, J., 1962: Velocity measurements in the deep water of the western North Atlantic: Summary. *J. Geophys. Res.*, **67**, 3173–3176.
- Curchitser, E. N., D. B. Haidvogel, and M. Iskandarani, 2001: Transient adjustment of circulation in a midlatitude abyssal ocean basin with realistic geometry and bathymetry. *J. Phys. Oceanogr.*, **31**, 725–745.
- Demadron, D., and G. Weatherly, 1994: Circulation, transport and bottom boundary layers of deep currents in the Brazil Basin. *J. Mar. Res.*, **52**, 583–638.
- Döös, K., 1995: Interocean exchange of water masses. *J. Geophys. Res.*, **100**, 13 499–13 514.
- Edwards, C. A., and J. Pedlosky, 1995: The influence of distributed sources and upwelling on the baroclinic structure of the abyssal circulation. *J. Phys. Oceanogr.*, **25**, 2259–2284.
- , and —, 1998: Dynamics of nonlinear cross-equatorial flow. Part I: Potential vorticity transformation. *J. Phys. Oceanogr.*, **28**, 2382–2406.
- Hall, M. M., M. McCartney, and J. A. Whitehead, 1997: Antarctic Bottom Water flux in the equatorial western Atlantic. *J. Phys. Oceanogr.*, **27**, 1903–1926.
- Hallberg, R., and P. Rhines, 1996: Buoyancy-driven circulation in an

- ocean basin with isopycnals intersecting the sloping boundary. *J. Phys. Oceanogr.*, **26**, 913–940.
- Hogg, N., and W. B. Owens, 1999: Direct measurement of the deep circulation within the Brazil Basin. *Deep-Sea Res.*, **46**, 335–353.
- , P. Biscaye, W. Gardner, and W. J. Schmitz, 1982: On the transport and modification of Antarctic Bottom Water in the Vema Channel. *J. Mar. Res.*, **40**, 231–263.
- , W. Owens, G. Siedler, and W. Zenk, 1996: Circulation in the Deep Brazil Basin. *The South Atlantic, Present and Past Circulation*, M. Wefer, Ed., Springer, 249–260.
- , G. Siedler, and W. Zenk, 1999: Circulation and variability at the southern boundary of the Brazil Basin. *J. Phys. Oceanogr.*, **29**, 145–157.
- Holland, W. R., 1978: The role of mesoscale eddies in the general circulation of the ocean—Numerical experiments using a wind-driven quasi-geostrophic model. *J. Phys. Oceanogr.*, **8**, 363–392.
- , and L. B. Lin, 1975: On the generation of mesoscale eddies and their contribution to the oceanic general circulation. Part I: A preliminary numerical experiment. *J. Phys. Oceanogr.*, **5**, 642–657.
- , and P. B. Rhines, 1980: An example of eddy-induced ocean circulation. *J. Phys. Oceanogr.*, **10**, 1010–1031.
- Hsu, Y.-J., and A. Arakawa, 1990: Numerical modeling of the atmosphere with an isentropic vertical coordinate. *Mon. Wea. Rev.*, **118**, 1933–1959.
- Huang, R. X., and X. Jin, 2002: Deep circulation in the South Atlantic induced by bottom-intensified mixing over the midocean ridge. *J. Phys. Oceanogr.*, **32**, 1150–1164.
- Kawase, M., 1987: Establishment of deep ocean circulation driven by deep water production. *J. Phys. Oceanogr.*, **17**, 2294–2317.
- , and D. Straub, 1991: Spinup of source driven circulation in an abyssal basin in the presence of bottom topography. *J. Phys. Oceanogr.*, **21**, 1501–1514.
- LaCasce, J. H., 2000: Floats and f/H . *J. Mar. Res.*, **58**, 61–95.
- , and K. G. Speer, 1999: Lagrangian statistics in unforced barotropic flows. *Deep-Sea Res.*, **57**, 245–274.
- Ledwell, J. R., E. T. Montgomery, K. L. Polzin, L. C. St. Laurent, R. W. Schmitt, and J. M. Toole, 2000: Evidence for enhanced mixing over rough topography in the abyssal ocean. *Nature*, **403**, 179–182.
- Mauritzen, C., K. L. Polzin, M. S. McCartney, R. C. Millard, and D. E. West-Mack, 2002: Evidence in hydrography and density fine structure for enhanced vertical mixing over the Mid-Atlantic Ridge in the western Atlantic. *J. Geophys. Res.*, **107**, 3147, doi:10.1029/2001JC001114.
- McCartney, M. S., and R. A. Curry, 1993: Transequatorial flow of Antarctic Bottom Water in the western Atlantic Ocean: Abyssal geostrophy at the equator. *J. Phys. Oceanogr.*, **23**, 1264–1276.
- McDougall, T. J., 1987: Thermobaricity, cabbeling, and water-mass conversion. *J. Geophys. Res.*, **92**, 5448–5464.
- Mercier, H., and K. Speer, 1998: Transport of bottom water in the Romanche Fracture Zone and the Chain Fracture Zone. *J. Phys. Oceanogr.*, **28**, 779–790.
- , G. L. Weatherly, and M. Arhan, 2000: Bottom water throughflows at the Rio de Janeiro and Rio Grande Fracture Zones. *Geophys. Res. Lett.*, **27**, 1503–1506.
- Morris, M. Y., M. M. Hall, L. C. St. Laurent, and N. G. Hogg, 2001: Abyssal mixing in the Brazil Basin. *J. Phys. Oceanogr.*, **31**, 3331–3348.
- Nakano, H., and N. Suginohara, 2002: A series of middepth zonal flows in the Pacific driven by winds. *J. Phys. Oceanogr.*, **32**, 161–176.
- O'Dwyer, J., and R. G. Williams, 1997: The climatological distribution of potential vorticity over the abyssal ocean. *J. Phys. Oceanogr.*, **27**, 2488–2506.
- Osborn, T. R., 1980: Estimates of the local rate of vertical diffusion from dissipation measurements. *J. Phys. Oceanogr.*, **10**, 83–89.
- Pedlosky, J., 1987: *Geophysical Fluid Dynamics*. 2d ed. Springer, 710 pp.
- , 1992: The baroclinic structure of the abyssal circulation. *J. Phys. Oceanogr.*, **22**, 652–659.
- , 1994: Ridges and recirculations—Gaps and jets. *J. Phys. Oceanogr.*, **24**, 2703–2707.
- , 1996: *Ocean Circulation Theory*. Springer, 453 pp.
- , 2001: Steady baroclinic flow through ridges and narrow gaps. *J. Phys. Oceanogr.*, **31**, 2418–2440.
- Polzin, K. L., J. M. Toole, J. R. Ledwell, and R. W. Schmitt, 1997: Spatial variability of turbulent mixing in the abyssal ocean. *Science*, **276**, 93–96.
- Reid, J. L., 1989: On the total geostrophic circulation of the South Atlantic Ocean: Flow patterns, tracers, and transports. *Progress in Oceanography*, Vol. 23, Pergamon, 149–244.
- Sandwell, D., S. Gille, J. Orcutt, and W. Smith, 2003: Bathymetry from space is now possible. *Eos, Trans. Amer. Geophys. Union*, **84**, 37.
- Sielicki, A., and M. G. Wurtele, 1970: The numerical integration of the non-linear shallow-water equations with sloping boundaries. *J. Comput. Phys.*, **6**, 219–236.
- Smith, W. H. F., and D. T. Sandwell, 1997: Global seafloor topography from satellite altimetry and ship depth soundings. *Science*, **277**, 1956–1962.
- Spall, M. A., 1994a: Mechanism for low-frequency variability and salt flux in the Mediterranean salt tongue. *J. Geophys. Res.*, **99**, 10 121–10 129.
- , 1994b: Wave-induced abyssal recirculations. *J. Mar. Res.*, **52**, 1051–1080.
- , 2001: Large-scale circulations forced by localized mixing over a sloping bottom. *J. Phys. Oceanogr.*, **31**, 2369–2384.
- Speer, K. G., and W. Zenk, 1993: The flow of Antarctic Bottom Water into the Brazil Basin. *J. Phys. Oceanogr.*, **23**, 2667–2682.
- Stephens, J. C., and D. P. Marshall, 2000: Dynamical pathways of Antarctic Bottom Water in the Atlantic. *J. Phys. Oceanogr.*, **30**, 622–640.
- St. Laurent, L., J. M. Toole, and R. W. Schmitt, 2001: Buoyancy forcing by turbulence above rough topography in the abyssal Brazil Basin. *J. Phys. Oceanogr.*, **31**, 3476–3495.
- Stommel, H., and A. B. Arons, 1960: On the abyssal circulation of the World Ocean. Part I: Stationary planetary flow patterns on a sphere. *Deep-Sea Res.*, **6**, 140–154.
- Swallow, J. C., 1971: The Aries current measurements in the western North Atlantic. *Philos. Trans. Roy. Soc. London*, **270A**, 451–460.
- , and L. V. Worthington, 1957: Measurements of deep currents in the western North Atlantic. *Nature*, **179**, 1183–1184.
- Thierry, V., A.-M. Treguier, and H. Mercier, 2004: Numerical study of the annual and semi-annual fluctuations in the deep equatorial Atlantic Ocean. *Ocean Modell.*, **6**, 1–30.
- Thurnherr, A. M., and K. G. Speer, 2003: Boundary mixing and topographic blocking on the Mid-Atlantic Ridge in the South Atlantic. *J. Phys. Oceanogr.*, **33**, 848–862.
- Treguier, A. M., N. G. Hogg, M. Maltrud, K. Speer, and V. Thierry, 2003: The origin of deep zonal flows in the Brazil Basin. *J. Phys. Oceanogr.*, **33**, 580–599.
- Weatherly, G., M. Arhan, H. Mercier, and W. Smethie, 2002: Evidence of abyssal eddies in the Brazil Basin. *J. Geophys. Res.*, **107**, 3027, doi:10.10129/2000JC000648.
- Williamson, J., 1980: Low-storage Runge–Kutta schemes. *J. Comput. Phys.*, **35**, 48–56.
- Wüst, G., 1935: Schichtung und Zirkulation des Atlantischen Ozeans. Die Stratosphäre, *Wissenschaftliche Ergebnisse der Deutschen Atlantischen Expedition auf dem Forschungsschiff "Meteor" 1925–1927*, Vol. 1, 180 pp.
- Yang, J., and J. F. Price, 2000: Water-mass formation and potential vorticity balance in an abyssal ocean circulation. *J. Mar. Res.*, **58**, 789–808.
- Zenk, W., G. Siedler, B. Lenz, and N. Hogg, 1999: Antarctic Bottom Water flow through the Hunter Channel. *J. Phys. Oceanogr.*, **29**, 2785–2801.